Biophysical Journal Volume 78 June 2000 3048–3071

Comparative Single-Molecule and Ensemble Myosin Enzymology: Sulfoindocyanine ATP and ADP Derivatives

Kazuhiro Oiwa,* John F. Eccleston,† Michael Anson,† Mahito Kikumoto,* Colin T. Davis,† Gordon P. Reid,† Michael A. Ferenczi,† John E. T. Corrie,† Akira Yamada,* Haruto Nakayama,* and David R. Trentham†

*Kansai Advanced Research Center, Communications Research Laboratory, Kobe 651-2492, Japan, and †National Institute for Medical Research, London NW7 1AA, United Kingdom

ABSTRACT Single-molecule and macroscopic reactions of fluorescent nucleotides with myosin have been compared. The single-molecule studies serve as paradigms for enzyme-catalyzed reactions and ligand-receptor interactions analyzed as individual stochastic processes. Fluorescent nucleotides, called Cy3-EDA-ATP and Cy5-EDA-ATP, were derived by coupling the dyes Cy3.29.OH and Cy5.29.OH (compounds XI and XIV, respectively, in Mujumdar et al. (1993, *Bioconjug. Chem.* 4:105–111)) with 2′(3′)-*O*-[*N*-(2-aminoethyl)carbamoyl]ATP (EDA-ATP). The ATP(ADP) analogs were separated into their respective 2′- and 3′-*O*-isomers, the interconversion rate of which was 30[OH^-] s^{-1} (0.016 h^{-1} at pH 7.1) at 22°C. Macroscopic studies showed that 2′(3′)-*O*-substituted nucleotides had properties similar to those of ATP and ADP in their interactions with myosin, actomyosin, and muscle fibers, although the ATP analogs did not relax muscle as well as ATP did. Significant differences in the fluorescence intensity of Cy3-nucleotide 2′- and 3′-*O*-isomers in free solution and when they interacted with myosin were evident. Single-molecule studies using total internal reflection fluorescence microscopy showed that reciprocal mean lifetimes of the nucleotide analogs interacting with myosin filaments were one- to severalfold greater than predicted from macroscopic data. Kinetic and equilibrium data of nucleotide-(acto)myosin interactions derived from single-molecule microscopy now have a biochemical and physiological framework. This is important for single-molecule mechanical studies of motor proteins.

INTRODUCTION

Measurement of the kinetics of an enzyme-catalyzed reaction at the level of a single molecule in an aqueous environment is a landmark in biophysics (Funatsu et al., 1995; Lu et al., 1998; Nie and Zare, 1997; Weiss, 1999; Xie and Trautman, 1998). The approach, based on observing the fluorescence of a substrate or cofactor when bound to immobilized enzyme, lends itself in principle to the analysis of other biological mechanisms, such as ligand-receptor and protein-DNA interactions. The reaction chosen by Funatsu et al. (1995) was the hydrolysis of a fluorescent ATP analog by the motor protein myosin. Over the past few years analysis of elementary steps of individual myosin molecules has provided convincing evidence about the nature of force development, motility, and work output in muscle and nonmuscle cells (Finer et al., 1994; Harada et al., 1987, 1990; Ishijima et al., 1994, 1998; Kron and Spudich, 1986; Mehta et al., 1999; Molloy et al., 1995; Toyoshima et al., 1987, 1990; Uyeda et al., 1990; Veigel et al., 1999; Warshaw et al., 1998). An important reason for analyzing nucleotide hydrolysis at the single-molecule level is that it opens up new approaches to the study of mechanochemical energy transduction in the myosin superfamily.

The advance made by Funatsu et al. (1995) raises a number of points, some of which are fundamental to the development of single-molecule studies for probing biological mechanisms. We need to know the extent to which individual stochastic versus ensemble (i.e., macroscopic) observations lead to identical results. Is there unique information about enzyme mechanisms that can be obtained by studying single enzyme molecules? Are there factors that derive from the state of the system under investigation (e.g., filamentous versus solubilized myosin)? In the single-molecule studies of Funatsu et al. (1995) myosin was adsorbed on a surface, while kinetic analysis of the myosin ATPase has generally been carried out with water-solubilized protein; the influence of the state of myosin therefore needs to be assessed. We address these issues by comparing kinetics of reactions involving myosin and fluorescent analogs of ATP in different systems. It is important to use analogs that closely mimic properties of ATP in its interactions with myosin and muscle, and therefore we have chosen to introduce the fluorophore on the 2′- or 3′- hydroxyl group of the ribose moiety of ATP (Alessi et al., 1992; Conibear et al., 1996; Cremo et al., 1990; Crowder and Cooke, 1987; Ferenczi et al., 1989; Hiratsuka, 1983, 1984; Sowerby et al., 1993; Tonomura, 1973; Woodward et al., 1991). The fluorescent ATP analog used by Funatsu et al. (1995), in contrast, was modified on the purine moiety of ATP, though in more recent work this group has used ribose-modified ATP analogs (Ishijima et al., 1998). Replacing the 2′- or 3′-hydroxyl group with probes has generally resulted in a

Received for publication 29 August 1999 and in final form 29 February 2000.

Address reprint requests to Dr. David R. Trentham, The Ridgeway, National Institute for Medical Research, Mill Hill, London NW7 1AA, UK. Tel.: 44-208-959-3666, X2074; Fax: 44-208-906-4419; E-mail: dtrenth@nimr.mrc.ac.uk.

Dr. Nakayama's present address is Planning Division, Communications Research Laboratory, 4-2-1 Nukui-Kitamachi, Koganei, Tokyo 184-8795, Japan.

0006-3495/00/06/3048/24 $2.00

mixture of compounds. If the link between the hydroxyl group and the probe is via a carboxylate ester there is relatively rapid isomerization at neutral pH between the resulting 2′- and 3′-*O*-esters of nucleotides (reviewed in Jameson and Eccleston, 1997). We have resolved this by synthesizing carbamoyl esters and showing that their isomerization is sufficiently slow for individual isomers to be separated. It has thus been possible to assess the effect of working with separated as opposed to mixed isomers of ATP analogs.

It is frequently advantageous in single-molecule kinetic studies to monitor at least two fluorophores. For example, besides detecting the myosin-bound substrate, the position of the myosin molecule itself had to be identified by Funatsu et al. (1995). Accordingly, we have used two fluorophores and compared their properties in ATP analogs. Part of the assessment involved measurement of their photobleaching properties. This is a crucial parameter, as monitoring the disappearance of a fluorophore from an enzyme bound to a surface is at the heart of many single-molecule experiments, and the rate of fluorescence loss from the surface due to photobleaching must be known. Like Funatsu et al. (1995) and Kuhlman and Bagshaw (1998), we have used the sulfoindocyanine dyes Cy3 and Cy5, developed by Mujumdar et al. (1993), which have large extinction coefficients and are fluorescent in the long-wavelength region of the visible spectrum.

The ability of Cy3 and Cy5 fluorescent ATP analogs to mimic ATP had to be tested in a variety of ways to assess their potential for energy transduction studies in muscle. This has been done through the delineation of the kinetics of elementary steps in the myosin- and actomyosin-catalyzed hydrolysis of the analogs in solution and the ability of the analogs to support muscle contraction and relaxation in permeabilized fibers, and by comparing their properties with those of ATP in in vitro motility assays.

Single-molecule kinetics have been monitored here, using the total internal reflection fluorescence (TIRF) technique (Axelrod et al., 1984; Funatsu et al., 1995). Conibear and Bagshaw (1996) have applied this approach, using myosin filaments adsorbed on a surface. We extend TIRF studies of the myosin triphosphatase and analyze the interaction between myosin and ADP analogs. The latter serves as a model for ligand-receptor interactions. We have compared ensemble and single-molecule triphosphatase studies of myosin and actomyosin directly with the TIRF technique and assessed the influence of steric interactions arising from binding of myosin filaments to a glass surface.

For these studies we have used the mixed isomers designated Cy3-EDA-ATP **1** and Cy5-EDA-ATP **2** and the corresponding diphosphates. The isomers of the Cy3-EDA-nucleotides have been separated and their structures assigned by NMR spectroscopy. This has enabled us to determine how the properties of 2′- and 3′-substituted nucleotides differ. Preliminary results have been reported in abstract form (Anson and Oiwa, 1997, 1998, 1999; Eccleston et al., 1996; Oiwa et al., 1995, 1996, 1997, 1998, 1999).

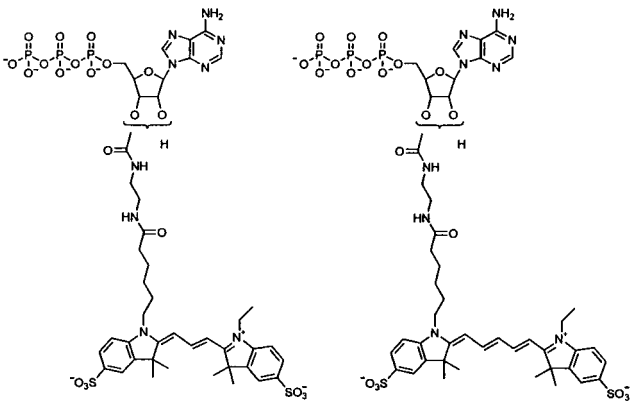

1 **2**

MATERIALS AND METHODS

Chemicals

The monosubstituted cyanine carboxylic acids Cy3.29.OH and Cy5.29.OH and their succinimidyl derivatives Cy3.29.OSu and Cy5.29.OSu were purchased from Biological Detection Systems (Pittsburgh, PA). 2′(3′)-*O*-(*N*-Methylanthraniloyl)ATP (mant-ATP) was synthesized and purified as described by Hiratsuka (1983) and Jameson and Eccleston (1997). Disuccinimidyl carbonate, dimethylformamide, ethylenediamine, high-performance liquid chromatography (HPLC)-grade acetonitrile, and pyridine were purchased from Aldrich Chemical Co. (Milwaukee, WI). Triethylammonium bicarbonate (TEAB) buffer was prepared by bubbling CO_2 through an ice-cold aqueous solution of redistilled triethylamine until the pH decreased to 7.6. All other reagents were of the highest available purity and were used without further treatment.

Synthesis and characterization of 2′-*O*-Ac-EDA-ADP and 3′-O-Ac-EDA-ADP

One hundred micromoles of the triethylammonium salt of EDA-ATP (2′(3′)-*O*-[*N*-(2-aminoethyl)carbamoyl]ATP) (Jameson and Eccleston, 1997) was stirred in 20 ml aqueous 40 mM $NaHCO_3$ and *N*-acetylated by the addition of 70 μl acetic anhydride. The reaction was maintained at pH 8.0 with solid $NaHCO_3$ at 20°C for 5 min. The mixed isomers were purified by DEAE-cellulose chromatography using a TEAB salt gradient and rotary evaporation of solvent followed by methanol evaporations to yield 26 μmol 2′(3′)-*O*-Ac-EDA-ATP as the triethylammonium salt. A sample was converted to its Na^+ salt for ^{1}H-NMR analysis (see below). The mixed triphosphates were hydrolyzed quantitatively to mixed isomers of 2′-*O*-Ac-EDA-ADP and 3′-*O*-Ac-EDA-ADP (formulae in Fig. 1) at pH 7 by myosin subfragment 1 (see Protein Preparations); the reaction was quenched by adjusting the pH to 4, and the solution was centrifuged to remove denatured subfragment 1. The equilibrium mixture of diphosphates (4.9 μmol in two runs, i.e., sufficient for ^{1}H-NMR analysis) was applied to a 300-mm-length × 7.8-mm-diameter semipreparative reverse-phase column (packed with Waters C_{18} 125 Å beads) equilibrated with aqueous 100 mM KH_2PO_4/K_2HPO_4 at pH 5.5 and 21°C. The diphosphates were eluted with water, and the isomers were separated with almost baseline resolution; subsequent analysis showed that the 2′-*O*-ester eluted first (see below).

Each isomer was evaporated to dryness in vacuo and dissolved in D_2O. ^{1}H-NMR spectroscopy (400 MHz) and analytical reverse-phase HPLC (Merck RP8; 100 × 3 mm column and same phosphate buffer) were used to characterize the isomers and to define their isomeric purity. Chemical shifts of the H-1′, H-2′, and H-3′ protons and the coupling constant of the H-1′ proton provided the basis of the NMR characterization (Fromageot et al., 1966; Onur et al., 1983). The H-4′ protons were also assigned. With this information the ^{1}H-NMR spectrum of the Na^+ salt of 2′(3′)-*O*-Ac-EDA-ATP was analyzed. The 2′-*O*-ester had δ 6.27 (d, J = 4.3 Hz, H-1′), 5.47 (H-2′), 4.41 (H-4′). H-3′ was not resolved from the HOD peak. The 3′-*O*-ester had δ 6.16 (d, J = 7.4 Hz, H-1′), 5.36 (H-3′), 5.00 (H-2′), 4.54 (H-4′). Spectra were recorded in D_2O at pD 6.9 with DSS (sodium 4,4-dimethyl-4-silapentane-1-sulfonate) as an internal reference.

Kinetics of isomerization between 2′-*O*-Ac-EDA-ADP and 3′-*O*-Ac-EDA-ADP

Pure 2′-*O*-Ac-EDA-ADP or 3′-*O*-Ac-EDA-ADP obtained from the analytical reverse-phase HPLC column in 100 mM KH_2PO_4/K_2HPO_4 at pH 5.5 was treated with 1 M K_2HPO_4, Tris, or Na_2CO_3 to bring the pH to 7.1, 8.4, or 9.4, respectively. These solutions were incubated at 22°C, and the isomerization rate was followed by quenching reaction samples (acidification to pH 5.5) and HPLC analysis using the same reverse-phase column. The isomerization was allowed to proceed to equilibrium, and the equilibrium constant was calculated from the ratio of the peak areas in the HPLC elution profile. When starting with 3′-*O*-Ac-EDA-ADP, k_{obs} (= k_{23} + k_{32}) (k_{23} and k_{32} are defined in Fig. 1) was calculated from the slope of the linear plot of $-\ln(1 - [2'\text{-}O\text{-Ac-EDA-ADP}]_t/[2'\text{-}O\text{-Ac-EDA-ADP}]_{t\to\infty})$ against time, t. Because $k_{23}/k_{32} = ([3'\text{-}O\text{-Ac-EDA-ADP}]_{t\to\infty}/[2'\text{-}O\text{-Ac-EDA-ADP}]_{t\to\infty})$ (i.e., the ratio of isomer concentrations at equilibrium), k_{23} and k_{32} could be calculated.

Synthesis of Cy3-EDA-ATP and Cy5-EDA-ATP

Cy3-EDA-ATP and Cy5-EDA-ATP were prepared by identical protocols as described by Jameson and Eccleston (1997). Typically a succinimidyl ester was formed from 4 μmol Cy3.29.OH or Cy5.29.OH and then condensed with 20 μmol EDA-ATP. The reaction was followed by thin-layer chromatography on silica plates (silica gel 60_{F254}; Merck, Germany) in a solvent of propan-2-ol:H_2O:NH_4OH (7:2:1, v/v). Cy3.29.OH (or Cy5.29.OH) had an R_f of 0.2 (0.3), with a minor impurity at R_f 0.8 in both cases. The reaction mixture containing crude Cy3-EDA-ATP or Cy5-EDA-ATP showed an intense pink (Cy3) or blue (Cy5) spot remaining at the origin and the presence of some Cy3.29.OH (or Cy5.29.OH) and other impurities. The presence of a new spot remaining at the origin indicates ribose modification of EDA-ATP by the fluorophore (Hazlett et al., 1993). The reaction mixture was purified on a DEAE-cellulose column (12 × 2 cm). The column was washed with 10 mM TEAB (pH 7.6) at a flow rate of 0.6 ml min^{-1} until no more pink (or blue) material was eluted. Then a linear gradient of 10 mM to 0.8 M TEAB was applied (total volume 600 ml). EDA-ATP eluted at 0.2 M TEAB, followed by a major peak with absorbance maxima at 260 nm and either 550 nm (for Cy3-EDA-ATP) or 650 nm (for Cy5-EDA-ATP) that eluted at ~0.4 M TEAB. The appropriate fractions were pooled and evaporated almost to dryness in vacuo. Residual triethylamine was removed by three additions and evaporations of methanol. The final material was redissolved in water and stored at −20°C. The ATP analogs were each obtained in 25% yield based on the initial weight of Cy3.29.OH or Cy5.29.OH.

Characterization of Cy3-EDA-ATP and Cy5-EDA-ATP

The absorbance spectra of Cy3.29.OH and Cy3-EDA-ATP in 50 mM Tris-HCl (pH 7.5) were recorded between 220 nm and 850 nm. Taking ε for the Cy3 chromophore to be 150,000 M^{-1} cm^{-1} at 552 nm (Mujumdar et al., 1993), a value of 6950 (± 1400 limit of error range) M^{-1} cm^{-1} at 260 nm was measured for Cy3.29.OH. Assuming that ε of the Cy3 chromophore in Cy3-EDA-ATP remains unchanged, and for adenosine, ε is 15,200 M^{-1} cm^{-1} at 260 nm, the molar ratio of Cy3 to adenosine in Cy3-EDA-ATP was calculated to be 1.04 (± 0.09) and is good evidence that Cy3-EDA-ATP contains equimolar amounts of Cy3 and adenosine. Corresponding values for Cy5-EDA-ATP were as follows: ε = 250,000 M^{-1} cm^{-1} (Mujumdar et al., 1993) and 8680 (± 2170) M^{-1} cm^{-1} for Cy5.29.OH at 650 nm and 260 nm, respectively, and the molar ratio of Cy5 to adenosine in Cy5-EDA-ATP was calculated from the absorbance spectrum to be 1.15 (± 0.19).

These molar ratios depend on reliable ε values of Cy3 and Cy5. Furthermore, the reported value of ε for Cy5.29.OH is exceptionally large, possibly exceeding the theoretical maximum for the intensity of the electronic absorption transition (assuming no intermolecular interactions such as chromophore stacking; see Discussion). Accordingly, ε for Cy5.29.OH was remeasured and found to be ≥218,000 M^{-1} cm^{-1} at λ_{max} 650 nm in aqueous solution at pH 7, using a dried and weighed sample of Cy5.29.OH. The value of 218,000 M^{-1} cm^{-1} is a lower limit because any colorless impurities in our sample would make the measured ε less than the true value. Except where noted otherwise, ε is taken to be 250,000 M^{-1} cm^{-1} at 650 nm (Mujumdar et al., 1993).

The fluorescence emission spectra of Cy3.29.OH and Cy3-EDA-ATP were identical, as were those of Cy5.29.OH and Cy5-EDA-ATP. Negative-ion fast-atom bombardment mass spectroscopy for Cy3-EDA-ATP and Cy5-EDA-ATP gave molecular ion peaks at m/z = 620.5 and 633.2, corresponding to doubly charged molecular masses (1241 and 1267) for $(\text{Cy3-EDA-ATP} + K^+)^{2-}$ and $(\text{Cy5-EDA-ATP} + K^+)^{2-}$, respectively.

Cy3-EDA-ATP was characterized by HPLC with a diode array (220–600 nm) or by 550-nm absorption for detection, using a reverse-phase column (Nova-Pak C_{18}, 150 × 3.9 mm; Waters). The flow was 1.5 ml min^{-1}, first isocratically for 2 min in 10 mM KH_2PO_4/K_2HPO_4 at pH 6.8 and then with a linear gradient of 1% (by volume) acetonitrile min^{-1} for 30 min. Cy3-EDA-ATP eluted after 15.6 min. Neither Cy3.29.OH nor other nucleotides (<1% level) were detected as contaminants. For Cy5-EDA-ATP conditions were identical, except that detection was by 260- and 650-nm absorption. Cy5-EDA-ATP eluted after 20.9 min. Cy5.29.OH (22.1 min) was a contaminant (<3%) and was the major impurity; no other nucleotides were detected (<1% level). Cy3 and Cy5 nucleotides were also routinely monitored by fluorescence, using HPLC, which had at least 100-fold greater sensitivity than absorption.

Synthesis of the ATP analogs was confirmed by showing that they were substrates for myosin subfragment 1 and yielded products, subsequently characterized as ADP analogs (see below), that were easily resolved by analytical HPLC from their parent ATP analogs.

Cy3-EDA-ATP was also characterized by ^{1}H-NMR spectroscopy (500 MHz); its structure was fully consistent with the ^{1}H spectrum. Ribose protons in the 2′ and 3′-*O* isomers were identified based on ribose proton assignments in 2′(3′)-*O*-Ac-EDA-ATP (see above). Selective TOCSY experiments (Xu and Evans, 1996) were used to confirm assignments in the isomer mixture by establishing the connectivity of ribose protons in each isomer. The H-2′ and H-4′ peaks of 2′-*O*-Cy3-EDA-ATP and the H-1′, H-2′, H-3′, and H-4′ peaks of 3′-*O*-Cy3-EDA-ATP were well resolved. The H-1′ and H-3′ peaks of the 2′ isomer overlapped with peaks from the Cy3 group and water, respectively. For 2′-*O*-Cy3-EDA-ATP the ^{1}H-NMR spectrum had δ 5.48 (H-2′) and 4.37 (H-4′), and 3′-*O*-Cy3-EDA-ATP had δ 6.10 (H-1′), 5.35 (H-3′), 5.00 (H-2′), and 4.46 (H-4′). The average intensity of the two resolvable ribose protons of 2′-*O*-Cy3-EDA-ATP relative to that of the four resolvable ribose protons of 3′-*O*-Cy3-EDA-ATP was 0.70. Thus the ratio of 3′-*O*-Cy3-EDA-ATP to 2′-*O*-Cy3-EDA-ATP was 1.43 in the mixture, which was then shown to be at equilibrium by HPLC analysis (see below).

Preparation of Cy3-EDA-ADP and Cy5-EDA-ADP

Cy3-EDA-ADP and Cy5-EDA-ADP were obtained by hydrolysis of the corresponding triphosphate (8.5 μM Cy3-EDA-ATP or 10 μM Cy5-EDA-ATP) catalyzed by rabbit skeletal muscle myosin (1 mg ml^{-1}) for 2 h in a stirred solution containing 1 mM $MgCl_2$, 0.2 mM dithiothreitol (DTT), and 10 mM Tris-HCl at pH 7.0 and 4°C. Myosin was removed by centrifugation, and the supernatant was stored at −20°C.

Cy3-EDA-ADP (100% yield) was analyzed by reverse-phase HPLC (Novapak C_{18}; 150 × 3.9 mm, 550 nm absorption) and eluted isocratically with acetonitrile:aqueous 10 mM K_2HPO_4/KH_2PO_4 at pH 6.8 (13:87 v/v) at 0.5 ml min^{-1}. Cy3-EDA-ADP eluted as two peaks (the putative 2′- and 3′-isomers) with almost baseline resolution, with retention times of 21.5 and 25.2 min. (In the same system Cy3-EDA-ATP eluted as a poorly resolved doublet with retention times of 17.3 and 18.7 min.) Cy5-EDA-ADP (100% yield) was analyzed using the same HPLC conditions but monitored by 650-nm absorption. The isomers of Cy5-EDA-ADP eluted as a well-resolved doublet with retention times of 20.2 and 21.5 min. (Under these conditions Cy5-EDA-ATP eluted as a doublet with retention times of 17.5 and 18.2 min.)

Separation and isomerization of 2′-*O*-Cy3-EDA-ATP and 3′-*O*-Cy3-EDA-ATP

The isomers of Cy3-EDA-ATP were separated on a 10-nmol scale by HPLC using the Nova-Pak C_{18} column with absorbance detection at 550 nm. Samples were eluted isocratically at 1.5 ml min^{-1} in acetonitrile: aqueous 100 mM TEAB at pH 7.4 and 22°C (1:10 by volume). The two isomers eluted as a doublet (area ratio of 1:1.4) with peak retention times of 31 and 35 min. The solution from each peak was evaporated to dryness in vacuo, and the solid was redissolved in water and stored at −80°C. Samples from each peak were analyzed on the same HPLC column, but using fluorescence detection (550 nm excitation, 565 nm emission). The first peak, designated isomer I, was 100% pure, and the second peak, isomer II, was 97% pure (3% contamination by isomer I).

The intensity ratio of the fluorescence of the leading peak (isomer I) to that of isomer II was 0.65. Noting that the fluorescence of isomer II is 92% that of isomer I (see below), the molar ratio of isomer I to isomer II is 0.65/0.92 = 0.71, showing that isomer I is 2′-*O*-Cy3-EDA-ATP and isomer II is 3′-*O*-Cy3-EDA-ATP. That the sample of 2′-*O*- and 3′-*O*-Cy3-EDA-ATP used in the NMR experiment had reached equilibrium was checked by incubating the mixture at pH 10 and 22°C for 3 h (estimated equilibration rate of 2.5 h^{-1}; see Results) and analyzing by HPLC. The fluorescence ratio of the 2′-*O*-Cy3-EDA-ATP peak to that of 3′-*O*-Cy3-EDA-ATP was identical (0.65) before and after the incubation. This establishes that the sample analyzed by NMR was at equilibrium and that, from the H′ peak intensities, the equilibrium constant (analogous to k_{23}/k_{32}) for the Cy3 nucleotides is 1.43.

The equilibration rate of 2′-*O*-Cy3-EDA-ATP and 3′-*O*-Cy3-EDA-ATP isomers was measured at 20°C by the addition of 0.2 M 3-(4-morpholino)-propanesulfonic acid (MOPS) adjusted to pH 7.2 with aqueous KOH or by the addition of 0.5 M $NaHCO_3$ adjusted to pH 9.6 with NaOH, and monitoring the reaction by HPLC. Whether isomerization occurs during hydrolysis catalyzed by myosin subfragment 1 was tested by incubating 5 μM 2′-*O*-Cy3-EDA-ATP with 100 nM subfragment 1 in 100 mM KCl, 5 mM $MgCl_2$, 1 mM DTT, and 50 mM Tris adjusted to pH 7.5 with HCl at 20°C. After reaction times of up to 8 min, aliquots of the reaction mixture were quenched in acid and analyzed under the same HPLC conditions that also separated the two isomers of Cy3-EDA-ADP.

Preparation and separation of 2′-*O*-Cy3-EDA-ADP and 3′-*O*-Cy3-EDA-ADP

Cy3-EDA-ATP (31 nmol) was hydrolyzed to Cy3-EDA-ADP as described above. The hydrolysis was monitored by reverse-phase HPLC (as in Preparation of Cy3-EDA-ADP and Cy5-EDA-ADP). When all of the Cy3-EDA-ATP had been hydrolyzed to Cy3-EDA-ADP, the solution was applied to the HPLC column. The two peaks, the first of 2′-*O*-Cy3-EDA-ADP and the second of 3′-*O*-Cy3-EDA-ADP, were collected. A sample from each peak was analyzed by the same HPLC system; the 2′ isomer was 100% pure, whereas the 3′ isomer was 98% pure (and contained 2% 2′ isomer). The remainder of each peak was evaporated to dryness in a Speedvac SVC100 (Savent) apparatus and then taken up in the original volume of water. The two solutions of Cy3-EDA-ADP isomers therefore each contained 10 mM potassium phosphate at pH 6.8.

Protein preparations

Rabbit skeletal muscle myosin and heavy meromyosin were prepared essentially as described by Margossian and Lowey (1982), and myosin subfragment 1 was prepared according to the method of Weeds and Taylor (1975). F-actin was prepared from acetone powder by the method of Pardee and Spudich (1982). For measurements in the microscope, F-actin was stabilized against depolymerization at low concentrations with phalloidin or, where visualization by fluorescence was required, with rhodamine-labeled phalloidin (Faulstich et al., 1988). Concentrations of myosin, heavy meromyosin, and subfragment 1 were determined from $A_{280\ nm}$ values for 1 mg ml^{-1} of 0.53, 0.65, and 0.79 cm^{-1} respectively, and the concentration of actin was determined from $A_{290\ nm} - A_{310\ nm}$ of 0.62 cm^{-1}.

Synthetic bipolar filaments of rabbit skeletal muscle myosin for TIRF studies were prepared by slowly diluting a myosin solution, initially 1 ml at a concentration of 50 μg ml^{-1} in 0.5 M KCl, 2 mM $MgCl_2$, 1 mM DTT, and 10 mM piperazine-*N,N*′-bis(2-ethanesulfonic acid) (PIPES) adjusted with KOH to pH 7.0 at 4°C, into 7.5 ml of the same buffer but containing 0.08 M KCl (Nagashima, 1986). The myosin filaments were further diluted in the same buffer to a final concentration of 2 μg ml^{-1} for infusion into the microscope observation chamber. Electron micrographs with negative staining showed that the length of the filaments ranged from 1.6 to 3.2 μm with an average of 2.6 ± 0.5 μm (mean ± SD, n = 83).

Labeling of myosin with Cy3.29.OSu and Cy5.29.OSu

To measure the photobleaching rates of Cy3 and Cy5 fluorophores under aqueous conditions it was necessary to immobilize fluorophores on myosin filaments to prevent exchange with free molecules in solution. Model myosin filaments were made using the succinimidyl esters of the dyes to couple covalently but nonspecifically to the constituent monomeric myosin. One milliliter of myosin solution at 5 mg ml^{-1} in 0.5 M KCl, 20 mM KH_2PO_4/K_2HPO_4 at pH 6.8 was added to 0.1 ml of 1 M sodium carbonate (pH 9.3) followed by 0.2 mg of either the Cy3.29.OSu or Cy5.29.OSu reagent. The reaction mixture was incubated at 4°C for 1 h with gentle stirring, then diluted 20-fold into 2 mM $MgCl_2$, 1 mM DTT, and 20 mM PIPES (adjusted to pH 7.0 with KOH) to form myosin filaments. The labeled myosin filaments were separated from unconjugated dye by low-speed centrifugation followed by resuspension, washing at pH 7, and further centrifugation. Molar concentrations of dye and myosin were calculated from the absorbance of the labeled myosin solution (ϵ 150,000 M^{-1} cm^{-1} at 550 nm for Cy3.29.OH, 250,000 M^{-1} cm^{-1} at 650 nm for Cy5.29.OH and 275,000 M^{-1} cm^{-1} at 280 nm for myosin; from $A_{280\ nm}$; see previous section). The molecular ratios of dye to myosin were ~10:1. Filaments suitable for analysis by TIRF were formed from the labeled myosin as described for unlabeled myosin.

Interaction of Cy3-EDA-ATP and Cy5-EDA-ATP with myosin subfragment 1

Stopped-flow measurements were carried out using a Hi-Tech Scientific SF61-MX instrument (Salisbury, UK) in the single-push fluorescence

mode, and records were analyzed, generally as single exponential decays, using Hi-Tech software or Origin 5. The relatively small Stokes shift in Cy3 and Cy5 fluorescence necessitated careful choice of excitation and emission wavelengths. A quartz-halogen lamp was used with monochromatic excitation at 520 and 600 nm for Cy3 and Cy5, respectively. These wavelengths correspond to shoulders on the absorption spectra 40–50 nm to the blue of the maxima (Mujumdar et al., 1993). Emitted light was transmitted through a Wratten 21 cutoff filter (0.1 and 50% transmission at 535 and 555 nm, respectively) to record Cy3 fluorescence and through a Wratten 70 cutoff filter (0.1 and 50% transmission at 640 and 675 nm, respectively) to record Cy5 fluorescence. Mant-ATP fluorescence was detected by energy transfer from tryptophan in subfragment 1 (Woodward et al., 1991). Excitation was at 290 nm from a 75-W mercury-xenon lamp, and emitted light was transmitted through a Wratten 47B bandpass filter (430 nm, bandwidth 50 nm). Actosubfragment 1 dissociation by ATP analogs was monitored at 350 nm, using the light-scattering signal orthogonal to the incident beam. Experiments were carried out at 20°C in solvent A (Table 2) to allow direct comparison with rate constants obtained with ATP and mantATP (Woodward et al., 1991) or in solvent B (Table 2) to allow direct comparison with TIRF measurements. Except where otherwise noted, concentrations quoted are those after mixing in the flow cell.

Myosin subfragment 1 and its actin-activated Cy3-EDA-ATPase and Cy5-EDA-ATPase activities were measured at 20°C in a reaction solution of 1 mM $MgCl_2$, 0.2 mM DTT, typically 40 μM Cy3-EDA-ATP or Cy5-EDA-ATP, 10 mM Tris adjusted to pH 7.5 with HCl, with between 0 and 72 or 36 μM F-actin, respectively. The reaction was started by the addition of 0.1–0.5 μM subfragment 1 in the absence of actin and 0.02 μM subfragment 1 in its presence. Aliquots of the reaction solution were then taken and quenched with acid at intervals of 30 s and then centrifuged, and aliquots from these supernatants analyzed by reverse-phase HPLC (see above), using isocratic rather than gradient elution with a mobile phase of acetonitrile:aqueous 100 mM KH_2PO_4/K_2HPO_4 at pH 6.8 (13:87 v/v). From the ratios of the diphosphate to triphosphate peak areas the Cy3- and Cy5-EDA-ATPase rates were determined. Actin-activated subfragment 1 ATPase was measured as described above, using 1.36 mM ATP, except that anion exchange HPLC (Whatman SAX) was used to resolve ATP and ADP with absorbance monitored at 260 nm.

Muscle fiber preparation and physiological measurements

Single muscle fibers from the rabbit psoas muscle were dissected, permeabilized, and mounted between a force transducer and a motor as described by Thirlwell et al. (1994). Cy3(Cy5)-EDA-ATP and ATP were compared as substrates in fibers by measuring the force that they induced in activated isometric fibers at 2.4–2.6 μm sarcomere length, following protocols essentially as in Alessi et al. (1992). The kinetics of fiber relaxation and activation were likewise compared. The rates of relaxation from the activated isometric state were measured as in Alessi et al. (1992), as were the rates of activation from the relaxed state, as described in the next paragraph.

The efficacy of Cy3(Cy5)-EDA-ATP was also determined by measurements of maximum shortening velocity under zero load, using the slack-test method of Edman (1979) as described in Thirlwell et al. (1995), except that insufficient Cy3(Cy5)-nucleotides were available to obtain enough data for statistical analysis. The muscle fiber was initially incubated in relaxing solution at 20°C that contained Cy3(Cy5)-EDA-ATP or ATP, 15 mM EGTA, 10 mM $MgCl_2$, 1 mM glutathione, 60 mM *N*-tris-(hydroxymethyl)methyl-2-aminoethanesulfonic acid adjusted to pH 7.1 with KOH, and K^+ propionate to bring ionic strength to 0.15 M. The fiber was then transferred to a similar solution that also contained sufficient Ca^{2+} to give 32 μM free Ca^{2+}, and tension developed. When an isometric plateau was reached, the length of the muscle fiber was decreased to drop the force to zero. The muscle fiber shortened under zero-load conditions to take up the slack and then force redeveloped. The muscle length was reduced sufficiently to allow for a measurable shortening time at zero load. The muscle length was returned to the initial value 0.5 s later. The process was repeated twice with different extents of shortening. The maximum shortening velocity was calculated from the time taken for the fiber to take up the slack and the extent of shortening.

In vitro motility assay

The in vitro motility assay was carried out as described by Anson (1992) with the modifications described below. A nitrocellulose-coated coverslip formed the bottom of a 40-μl flow cell, and 100 μl of heavy meromyosin at 50 μg ml^{-1} was used to coat the surface. After washing, 10–20 nM F-actin, labeled and stabilized with rhodamine-phalloidin, was introduced and allowed to bind to the heavy meromyosin in rigor. Unbound F-actin was washed out, and the cell was flushed with motility buffer, 25 mM KCl, 4 mM $MgCl_2$, 1 mM EGTA, 0.5 mg ml^{-1} bovine serum albumin, 5 mM DTT, 25 mM HEPES adjusted to pH 7.5 with KOH, containing 100 μg ml^{-1} glucose oxidase, 20 μg ml^{-1} catalase, and 3–5 mg ml^{-1} glucose as an oxygen-depleting antifade mixture (Harada et al., 1990). The flow cell was transferred to an inverted epifluorescence microscope (Axiovert 35; Carl Zeiss Jena, Jena, Germany). Rhodamine fluorescence was excited either by the 546-nm line of a 100-W mercury arc lamp (HBO-100 W2) selected by a 546-nm interference filter (bandpass 8 nm) and a BG18 red-absorbing filter, or a 1-mW, 543-nm He-Ne laser (1674P; Uniphase, San Jose, CA). Imaging was via a 560-nm dichroic reflector and a 580-nm interference filter (bandwidth 30 nm; 560DRLP02 and 580DRF30; Omega Optical, Brattleboro, VT) by a Plan-Neofluar 40×, 1.3 NA oil-immersion objective (Carl Zeiss) through a 4× magnifying lens onto an intensified CCD TV camera (Darkstar 800; Photonic Science, Robertsbridge, UK). TV-rate (CCIR, 25 frames s^{-1}) images were rolling averaged over four frames by an image processor (Argus 10; Hamamatsu Photonics, Hamamatsu, Japan). The averaged image was stored with time-marking, using a time-date generator (VTG33; ForA, Tokyo, Japan) and an S-VHS (PAL) videotape recorder (BRS-800E; JVC, Yokohama, Japan). After focusing and recording actin filaments in rigor as a reference, we started motility on the microscope by perfusing into the flow cell 100 μl of motility buffer containing Cy5-EDA-ATP or, for reference, mant-ATP. All solutions were stored on ice, and the microscope stage and flow cell were stabilized at 25°C for the assays.

Measurement of F-actin velocity

Computer analysis of the video recordings was carried out in a manner similar to that used by Anson et al. (1995), but employing different video equipment. Videotapes of the F-actin movement were played back off-line by the BRS-800E VCR, and the images were converted in real time by a CVR22 digital standards converter (Snell and Wilcox, Petersfield, UK) from PAL (25 frames s^{-1}, 625 lines) to NTSC (30 frames s^{-1}, 525 lines). This allowed digitization of the images with a VP110 video processor (Motion Analysis, Santa Rosa, CA) and their automatic tracking by computer, using the Expert Vision system (Motion Analysis) running on a 486DX2 66 MHz PC. In view of the low actin velocities (<1 μm s^{-1}) produced by the low concentrations of ATP analogs used, video frames were digitized at 1 frame s^{-1} (Homsher et al., 1992).

TIRF microscopy

The apparatus

The TIRF microscope was similar to that described by Funatsu et al. (1995). In some experiments including measurements of rates of photobleaching of Cy3- and Cy5-labeled myosin filaments, a fused-silica hemicylinder, 15 mm long and 15 mm in diameter, was used for total internal reflection of the excitation laser beam to establish the evanescent wave. In

later TIRF experiments, including measurements of single-molecule fluorescence, a trapezoidal prism of fused silica (5 mm thick with a 15-mm-square base, the two angled faces at 70°, and the top (11 × 15 mm) parallel to the base) was used. The two angled faces were antireflection-coated for wavelengths from 500 to 800 nm. Optical components were carefully cleaned with 1 M KOH and ethanol and protected from dust.

Flow cells and observation chambers were constructed in one of the following ways: two slivers of polycarbonate film 2 mm wide and 50 μm thick were placed ~5 mm apart on a glass coverslip 120–170 μm thick, which was fixed to the stage of an inverted microscope (Axiovert 100; Carl Zeiss). The hemispherical prism was then placed carefully on the polycarbonate spacers with its flat surface facing the coverslip. The space between the surface of the prism and the upper surface of the coverslip was used as a chamber (volume ~5 μl) for the observation of Cy3-EDA-ATP and Cy5-EDA-ATP on myosin filaments. Laser light (see below) after focusing with a lens with a focal length of 100 mm was passed into the hemicylinder, so the angle of incidence on the bottom surface was greater than the critical angle (66°) for a fused-silica/water interface. An elliptical spot of Gaussian distribution was produced, with approximate dimensions of 240 × 70 μm (1.3×10^{-8} m^2) at the e^{-2} intensity contour.

Alternatively, a flow cell was formed from two coverslips (15 × 15 mm) with 50-μm polycarbonate spacers between them. The lower glass coverslip was 120–170 μm thick, and the top surface was formed by a fused-silica coverslip (350 μm thick). After this flow cell (volume ~5 μl) was placed on the microscope, the base of the trapezoidal prism was optically contacted to the upper surface of the second coverslip, using glycerol (n 1.47) as a refractive index matching fluid. Laser light was focused with a lens with a 75-mm focal length that was perpendicular to one of the angled faces of the prism. This gave an angle of incidence at the fused-silica/water interface of 70° and produced a Gaussian elliptical spot with axes of ~150 × ~50 μm (6×10^{-9} m^2).

The evanescent wave (Axelrod et al., 1984) produced both in the hemicylinder arrangement and by use of the trapezoidal prism, at an angle of incidence of 70º, decayed exponentially from the silica-water interface with its intensity decreasing to e^{-2} of its maximum value at a depth of ~200 nm in the solution. Thus only fluorophores close to the interface were efficiently excited.

The temperature of the flow cell was monitored by an infrared detector and controlled by pumping a water-glycerol mixture (1:1 v/v) from a thermally controlled (−20 to 20°C) water bath through a copper pipe surrounding the flow cell mounting and a brass jacket surrounding the microscope objective similar to that described by Anson (1992). Early experiments (e.g., Fig. 8) were carried out at 25°C, as temperature control was by heating alone and hence was restricted to temperatures above the ambient temperature.

For the excitation of Cy3-EDA-ATP (and Cy3-EDA-ADP) fluorescence, a 15-mW single-line (514.5 nm) argon-ion laser (163; Spectra Physics, Mountain View, CA) or, for later experiments, a 50-mW single-line (532 nm) frequency-doubled Nd^{3+}:YAG laser (μ-Green laser; Uniphase) was used. To establish the evanescent field to excite Cy5-EDA-ATP, a continuous-wave dye laser (375B, Spectra Physics) pumped by a 5-W multiline argon-ion laser (2025-05; Spectra Physics), tunable from 615 to 745 nm with a maximum output power of 1.4 W at 650 nm, was used. The output of the dye laser was passed through a laser-line filter with a center wavelength of 630 nm and a bandwidth of 16 nm. In all cases plane-polarized laser beams were converted to circularly polarized beams by an appropriate quarter-wave plate, and the intensity was adjusted by means of attenuators placed in the beam.

Fluorescence was then collected by an objective lens (Plan-Neofluar 100× 1.3 NA; Carl Zeiss), through bandpass filters with a center wavelength of 575 nm and a bandwidth of 50 nm (HQ575/50X; Chroma Technology Corp., Brattleboro, VT) for Cy3-EDA-ATP or a center wavelength of 665 nm and a bandwidth of 65 nm (HQ 665/65X; Chroma Technology Corp.) for Cy5-EDA-ATP, to select dye fluorescence and cut excitation light. For Cy5, fluorescence was detected with an intensified CCD camera (C2400-87; Hamamatsu Photonics). For Cy3 fluorescence detection, the C2400 intensified CCD camera was preceded by a high-quantum-efficiency second image intensifier (VS4–1845; Video Scope International, Sterling, VA). This extra stage of optical preamplification increased the signal-to-noise ratio for single-molecule fluorescence by about threefold.

Images were processed with rolling averaging and contrast enhancement, using an Argus 20 image processor (Hamamatsu Photonics), and recorded on S-VHS videotape and simultaneously on a magnetooptical disk (LQ-4100A; Panasonic, Osaka, Japan) at a RS170 (NTSC) video rate of 30 frames s^{-1}. We used an eight-frame rolling average for dwell time determinations, resulting in a time resolution of 270 ms. The images stored on magnetooptical disks were analyzed off-line, using a frame-grabber to transfer data to a Macintosh computer running Image Analyst software (Automatrix, Middlesex, MA).

Two general classes of experiments were performed with the myosin filaments: those designed to establish the ensemble kinetic properties of the Cy3-EDA-ATPase and Cy5-EDA-ATPase of the adsorbed myosin filaments as opposed to myosin subfragment 1 in solution, and those that were single-molecule studies of the Cy3- and Cy5-nucleotides interacting with the filaments. In the former case Cy3- and Cy5-nucleotides bound to the filaments gave uniformly bright fluorescence images. Cy3- and Cy5-fluorescence away from the filament increased with nucleotide concentration; this background fluorescence was subtracted from that of the filaments and was generally more problematic at high Cy3-nucleotide concentrations.

In single-molecule experiments the fluorescence intensities of Cy3- and Cy5-EDA-ATP (ADP) bound to myosin filaments were analyzed using Image Analyst as follows. Images of individual filaments in video frames were recorded at relatively high concentrations of fluorescent analog (~50 nM for triphosphates and ~300 nM for diphosphates) at the end of a single-molecule experiment. These images were displayed and their positions recorded. Rectangles (typically 10 × 20 pixels, equivalent to 1.9 × 3.7 μm) enclosing each filament were drawn on the screen. The rectangles became spatial filters such that only pixels within each rectangle were analyzed. The spots from the single-molecule fluorescence were analyzed from the digital images by averaging pixel intensities over each of these preset rectangles. Corresponding fluorescence intensities from every video frame were stored on the computer's magnetic disk, and, as required, the variance of the intensity was calculated. In this way only fluorescence from the region around a myosin filament, in which the exact filament position could not otherwise be seen, was included in single-molecule experiments. Using the same procedure as described above, background intensity was estimated from nearby areas, defined by the same size rectangles but free of filaments. The video frames were also monitored by eye, for example, to assess the frequency at which discrete spots occurred on a filament as a function of nucleotide concentration.

The dwell times of the spots observed on myosin filaments were determined by measuring the duration that an individual Cy3- or Cy5-nucleotide remained bound to a myosin filament and so continued to produce a discrete fluorescent spot (as shown in Fig. 11). The recording time of the traces from which the distributions were derived was typically 15 min. As shown below, Cy3 fluorescence was more resistant to photobleaching than that of Cy5, so single-molecule kinetic studies are restricted to Cy3-nucleotides.

The distribution of dwell times was analyzed as the best fit to an exponential decay that is the expected behavior of the distribution of lifetimes of individual stochastic processes (Colquhoun and Hawkes, 1994). The fit of the exponential gives the first-order rate constant for the process under investigation and equals $1/\tau$, the reciprocal of the mean lifetime. The relationship between the distribution of lifetimes and macroscopic (ensemble) kinetics for single and multiple ion-channel recordings has been described in detail by Colquhoun and Hawkes (1994).

For measurements of the rate of photobleaching, synthetic filaments of Cy3- or Cy5-labeled myosin were attached to the flat surface of the hemicylinder and illuminated by evanescent waves at various powers. The 532-nm Nd^{3+}:YAG laser was used for Cy3-labeled filaments, and the dye

laser with the 630-nm laser-line filter was used for Cy5-labeled filaments. The laser was focused by the 100-mm lens into the hemicylinder as described above, producing the 240 × 70 μm (1.3×10^{-8} m^2) spot. A photon-counting photomultiplier tube, type R3550 (Hamamatsu Photonics) with a bialkali photocathode for Cy3 fluorescence or type H3460–53 (Hamamatsu Photonics) with a multialkali (Na-K-Sb-Cs) photocathode for Cy5, was attached to the 35-mm camera port of the microscope. The extra magnification, 2.5×, together with the 100× from the objective lens gave a field of view on the observation surface with a diameter of nearly 90 μm. Thus fluorescence from many myosin filaments was integrated by the photomultiplier. The rate of change of fluorescence intensity was monitored, and the photoelectrons were counted in 0.5-s time bins.

Manipulations of myosin filaments and solutions in the flow cells

Five microliters of aqueous solution containing 2 μg ml^{-1} synthetic myosin filaments in solvent B (Table 2), together with 100 μg ml^{-1} glucose oxidase, 20 μg ml^{-1} catalase, and 3 mg ml^{-1} glucose for oxygen depletion, were introduced into the chamber. Myosin filaments spontaneously attached to the fused-silica surface, where they could be observed. Twenty-microliter aliquots of the above solution (without myosin) containing Cy3- or Cy5-labeled nucleotides were injected into one side of the chamber with a pipette and drawn from the opposite side with a piece of filter paper. In photobleaching experiments Cy3- or Cy5-labeled myosin filaments rather than unlabeled filaments were used. Phalloidin-stabilized actin filaments were introduced for studies of actin-activated Cy3(Cy5)-EDA-ATPase. Control assays of actin binding were performed by incubating rhodamine-phalloidin actin filaments with immobilized myosin filaments; several actin filaments were observed in a conventional epifluorescence microscope to bind to each myosin filament. Actin was not released from the myosin filaments by 50 nM Cy5-EDA-ATP, a typical concentration used in experiments. With the addition of excess ATP, most actin filaments became detached and were washed from the myosin filaments.

Kinetics of solution exchange in the flow cell

As ATP was used to dissociate Cy3- and Cy5-EDA-nucleotides from myosin filaments (Figs. 8 and 9), it was important to establish that the rate of introducing ATP exceeded that of the dissociation. Furthermore, the rate of introduction of a new solution had to be measured near the glass surface from which the Cy3 or Cy5 fluorescence originated rather than from the bulk solution. This was done by first filling the cell with nonfluorescent solution; then 1 μM Cy5.29.OH was allowed to perfuse in rapidly, and its fluorescence was monitored using evanescent wave excitation (Fig. 8 *B, inset*). Cy5 fluorescence increased linearly with time for 35% of the overall signal; thereafter the signal was nonlinear and was 90% complete in 1.2 s. The 35% change was reached 300 ms from the time when the Cy5 fluorescence began to increase. ATP (1 mM) was used to displace the ATP analogs, so the initial rate of change of ATP concentration was 1.2 μM ms^{-1}. It follows that [ATP] will be >100 μM by 100 ms. The association rate constant of ATP binding to myosin is 1.8 μM^{-1} s^{-1} (Table 1), so the introduced ATP will have saturated any nucleotide-free ATPase site on the myosin filament by 100 ms. (The K_m of ATP for myosin is ~50 nM.) Consequently the fluorescence records in Figs. 8 and 9 reflect Cy5- and Cy3-EDA-nucleotide displacements because these processes are slow enough not to be limited by the rate of ATP introduction into the flow cell.

Data analysis and curve fitting

Statistical data analysis, nonlinear curve fitting, and graphical presentation were carried out with either Origin 5 (Microcal Software, Northampton, MA) or Sigmaplot 4.0 (SPSS, Chicago, IL) software running on IBM Pentium PC platforms. Critical analyses were checked using both programs. Standard deviations (SD) are quoted as mean ± SD. However, in several of the stopped-flow experiments there was insufficient cyanine nucleotide to repeat experiments with different subfragment 1 preparations. In these cases we estimate that the maximum range of the rate constant k was from 0.7 k to 1.4 k.

RESULTS

Interconversion kinetics of 2′- and 3′-*O*-Ac-EDA-ADP

Fig. 1 illustrates an HPLC analysis of an experiment at pH 9.4 and 22°C recording the time course of conversion from 3′-*O*-Ac-EDA-ADP to 2′-*O*-Ac-EDA-ADP. Measurements (not shown) were also made at 22°C, starting from the

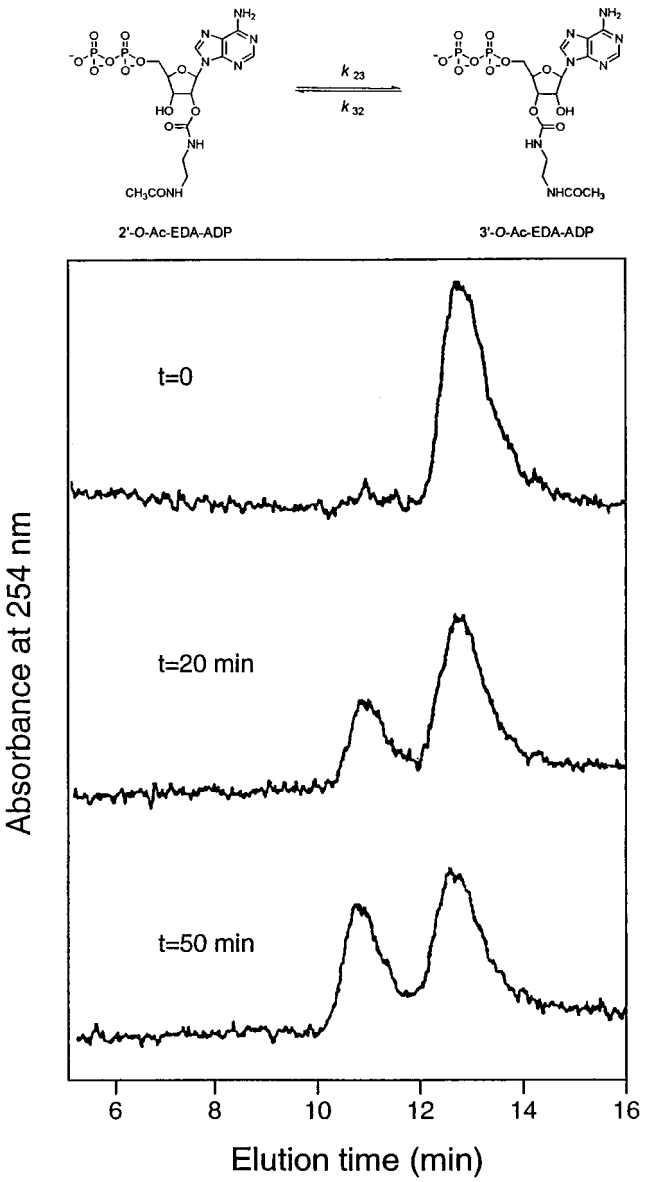

FIGURE 1 Equilibration of 3′-*O*-Ac-EDA-ADP to a mixture of the 2′- and 3′-*O*-esters. HPLC absorbance records at 254 nm after the incubation of 3′-*O*-Ac-EDA-ADP for times as indicated at pH 9.4 and 22°C.

3′-*O*-ester at pH 7.1 and 8.4 and from the 2′-*O*-ester at pH 9.4. Based on the isomerization scheme in Fig. 1, values of k_{23} are 0.010, 0.14, and 1.40 h^{-1}, and values of k_{32} are 0.007, 0.098, and 1.00 h^{-1} at pH 7.1, 8.4, and 9.4, respectively. The mean value of the equilibrium constant for the isomerization (k_{23}/k_{32}) equals 1.4 when it is measured from the equilibrium proportions of [3′-*O*-Ac-EDA-ADP] to [2′-*O*-Ac-EDA-ADP]. The isomerization rate, expressed as ($k_{23} + k_{32}$), is proportional to [OH^-] over the pH range 7.1 to 9.4 and equals 30[OH^-] s^{-1}.

The chemistry of Cy3-EDA- and Cy5-EDA-nucleotides

Separation of 2′- and 3′-isomers was achieved on a 10-nmol scale for Cy3-EDA-ATP and a 30-nmol scale for Cy3-EDA-ADP. The Cy5-EDA-ADP isomers were similarly separated but, unlike the Cy3 isomers, were not subjected to further experiments. For both Cy3- and Cy5-EDA-ATP (as for the 2′(3′)-*O*-Ac-EDA-ADP) the earlier eluting isomer peak had the smaller absorption (range 1:1.4 to 1:1.5), and for Cy3-EDA-ATP it was identified by ^{1}H-NMR as the 2′-*O*-isomer. Isomerization rates were measured for 2′-*O*- and 3′-*O*-Cy3-EDA-ATP. At pH 7.2 and pH 9.6 the rates were <0.01 h^{-1} and 1.0 h^{-1}, respectively, at 20°C. No isomerization was detected during the hydrolysis of 5 μM 2′-*O*-Cy3-EDA-ATP to 2′-*O*-Cy3-EDA-ADP by 100 nM subfragment 1 at 20°C and pH 7.5.

Fluorescence of 2′-*O*- and 3′-*O*-Cy3-EDA-ATP(ADP)

After isomer separation it was possible to compare the ratio of the fluorescence of 2′-*O*-Cy3-EDA-ATP and 3′-*O*-Cy3-EDA-ATP (assuming identical ϵ values). It was important to know this, as otherwise it would not be clear to what extent a fluorescence difference when the 2′- or 3′-isomer bound to myosin subfragment 1 in solution was due to a difference when the isomer was not bound. This in turn influences the analysis in TIRF experiments. At the emission peak 3′-*O*-Cy3-EDA-ATP fluorescence was 89% of that of 2′-*O*-Cy3-EDA-ATP in solvent A. In a further study the two isomers of Cy3-EDA-ADP were separated from a (nonequilibrium) mixture by HPLC and monitored using absorption and fluorescence HPLC detectors. The ratio of the absorption peaks was 1:1.72, and that of the fluorescent peaks was 1:1.59, indicating that the fluorescence of 3′-*O*-Cy3-EDA-ADP was 92% of that of 2′-*O*-Cy3-EDA-ADP.

Elementary processes of Cy3-EDA-ATPase and Cy5-EDA-ATPase activities

Data in Table 1 summarize the results obtained by analysis of the interaction of free myosin subfragment 1 in solution with Cy3- and Cy5-EDA-nucleotides in the presence and absence of actin. Most of the data in Table 1 are derived from mixed isomers; those from separated isomers are shown in brackets. Except for *ss* k_{cat}, results relating to subfragment 1 alone were obtained by transient kinetic methods as follows. The second-order association rate constant, k_{+1}, was calculated by measuring the dependence of the observed rate of Cy3 fluorescence increase (Fig. 2 *A*) or Cy5 fluorescence decrease (Fig. 2 *D*) on subfragment 1 concentration (0.5–5 μM) when the ATP analogs were mixed with subfragment 1 in excess. This yielded values for k_{+1} of 1.2 and 1.4 μM^{-1} s^{-1} for Cy3- and Cy5-EDA-ATP, respectively.

Under single turnover conditions (i.e., [subfragment 1] > [ATP analogue]) there is a characteristic formation and

TABLE 1 Rate constants of the interaction of Cy3-EDA-ATP and Cy5-EDA-ATP with myosin subfragment 1 at 20°C

$$M + NTP \overset{1}{\rightleftharpoons} M \cdot NTP \overset{2}{\rightleftharpoons} M \cdot NDP \cdot P_i \overset{3}{\rightleftharpoons} M \cdot NDP + P_i \overset{4}{\rightleftharpoons} M + NDP$$

Equilibrium and rate constants*	Cy3-EDA-ATP	Cy5-EDA-ATP	Mant-ATP†	ATP†
k_{+1} (μM^{-1} s^{-1})‡	1.2 (1.1, 1.1)¶	1.4	3.2	1.8
k_{+3} (s^{-1}) (k_{cat})‡,§	0.022 (0.080, 0.022)¶	0.035	0.04	0.06
k_{+4} (s^{-1})‡	1.3 (2.6, 1.7)¶	1.6	0.22	1.4
K_4 (μM)	2.6	2.4	0.10	0.9
ss k_{cat} (s^{-1})	0.056	0.034	0.04	0.055
Actin activation	$A \cdot M + NTP \overset{1'}{\rightleftharpoons} A + M \cdot NTP$			
K'_m (μM) (actin)	95	61	ND	34
V_{max} (s^{-1})	21	15	ND	16
k'_{+1} (μM^{-1} s^{-1})	0.95	0.93	3	2.7

*K_i, k_{+i}, and k_{-i} are equilibrium, forward, and reverse rate constants, respectively, of the *i*th step. The methods and conditions for the determination of rate constants are given under Materials and Methods and in the figure legends. Standard deviations (SDs), where measured, are recorded in Table 2 or the main text. NTP, nucleoside 5′-triphosphate; NDP, nucleoside 5′-diphosphate; *ss* k_{cat}, steady-state k_{cat}; ND, not determined.

†Millar and Geeves (1983), Trentham et al. (1976), Woodward et al. (1991) (K'_m and V_{max} for actin-activated ATPase, this work).

‡The fluorescence signals are dominated by transients of the 3′ isomers (see text).

§These rate constants are more correctly equal to $k_{+2}k_{+3}/(k_{+2} + k_{-2})$.

¶Rate constants in brackets are for the separated (2′, 3′) isomers of Cy3-EDA-ATP or Cy3-EDA-ADP.

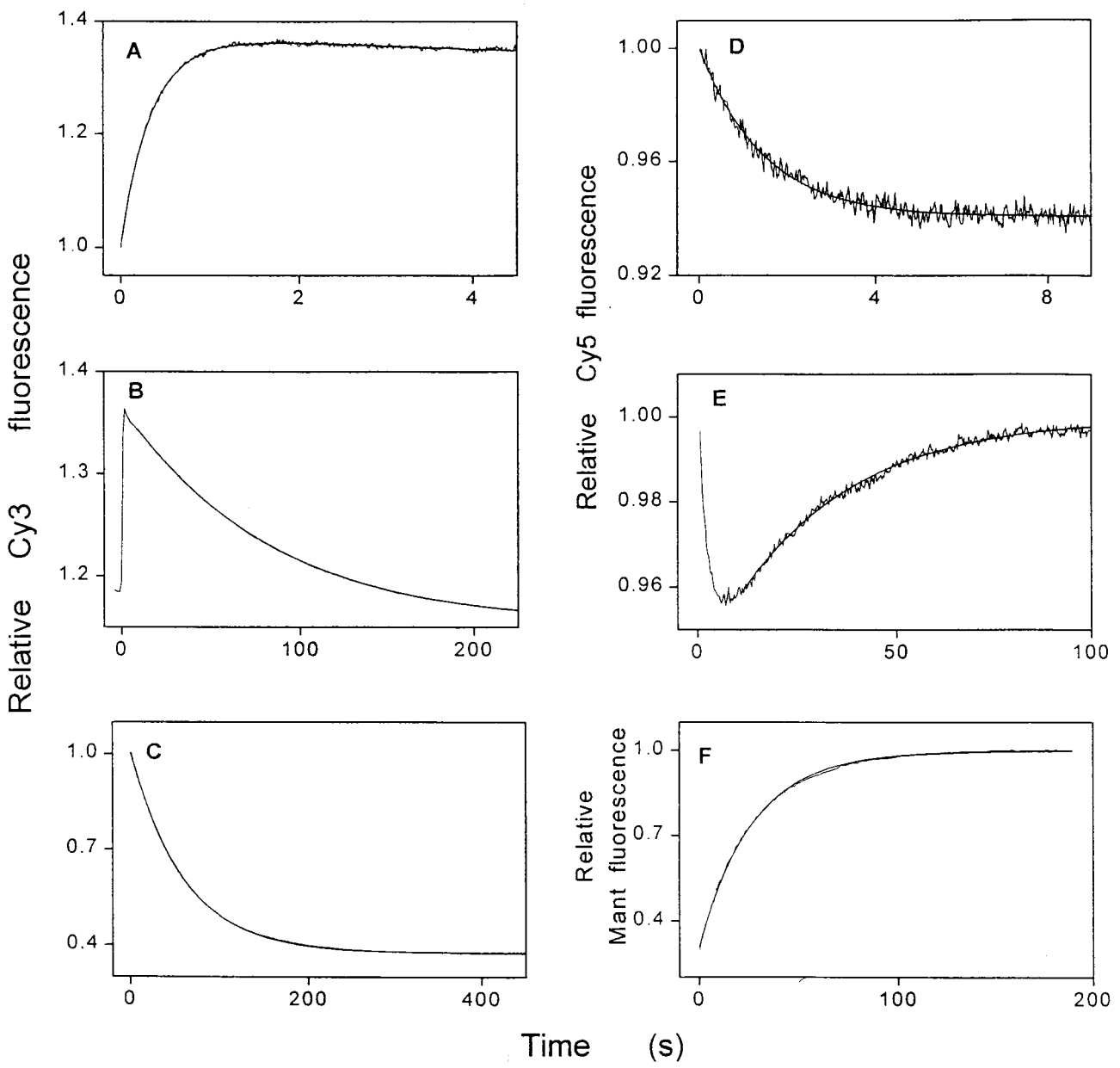

FIGURE 2 Stopped-flow fluorescence records of the interaction of Cy3-EDA-ATP and Cy5-EDA-ATP with subfragment 1. (*A* and *B*) 2.5 μM subfragment 1 mixed with 0.25 μM Cy3-EDA-ATP. (*C*) 0.5 μM subfragment 1 preincubated for <5 s with 1.0 μM Cy3-EDA-ATP and mixed with 50 μM ATP. (*D* and *E*) 1 μM subfragment 1 mixed with 0.4 μM Cy5-EDA-ATP. (*F*) 1 μM subfragment 1 preincubated for <5 s with 2 μM Cy5-EDA-ATP and mixed with 20 μM mant-ATP. Nonlinear least-squares fit of single (double in *A*) exponentials is drawn through the data with rate constants of (*A*) 2.9 s^{-1} (second phase 0.018 s^{-1}), (*B*) 0.0125 s^{-1}, (*C*) 0.017 s^{-1}, (*D*) 0.71 s^{-1}, (*E*) 0.034 s^{-1}, and (*F*) 0.038 s^{-1}. Note that the fluorescence decay in *B* has an unexplained phase of small amplitude that precedes the main decay phase. Reaction chamber concentrations are listed (hence preincubations in *C* and *F* were carried out at double the indicated concentrations). The fluorescence of Cy3 and Cy5 is recorded in *A–E*. In *F* mant fluorescence is recorded as described in Materials and Methods. Reactions were carried out at 20°C in solvent A (Table 2). Zero time is the time at which flow stopped after solution mixing.

decay of an intermediate. This is the same as the steady-state intermediate of the triphosphatase reaction when the ATP analog is in excess (Bagshaw and Trentham, 1973). This decay was evident as a Cy3 fluorescence decrease (Fig. 2 *B*) and a Cy5 fluorescence increase (Fig. 2 *E*) in the cases of Cy3-EDA-ATP and Cy5-EDA-ATP, respectively. The exponential decay rates were independent of subfragment 1 concentration and were equated with k_{cat} (or k_{+3}; more correctly, $k_{+2}k_{+3}/(k_{+2} + k_{-2})$) (Table 1), because at least in the case of ATP, the ATP cleavage step is reversible (Bagshaw and Trentham, 1973).

Several checks were made on the above results and their interpretation. The rapid phase associated with Cy5-EDA-ATP binding to subfragment 1 was also observed as a 10%

protein fluorescence decrease (data not shown) that contrasts with the 20% protein fluorescence increase on ATP binding. As a second test each nucleotide analog was added to subfragment 1 and within 5 s mixed with a 100-fold excess of ATP (Cy3 experiment) or mant-ATP (Cy5 experiment). (The use of mant-ATP rather than ATP and monitoring mant fluorescence for the Cy5-EDA-ATP experiments gave an improved signal-to-noise ratio.) Under these conditions the Cy3- or Cy5-EDA-ATP bound to subfragment 1 will be displaced from its steady-state intermediate. As predicted, the exponential rates in Fig. 2, *C* and *F*, matched those in Fig. 2, *B* and *E*, respectively. Finally Mg^{2+}-dependent subfragment 1 Cy3-EDA-ATPase and Cy5-EDA-ATPase activities (called *ss* k_{cat} in Table 1) were measured using a steady-state assay used for the actin-activated analysis (see Materials and Methods); rates were 0.030 and 0.018 μmol min^{-1} (mg subfragment 1)$^{-1}$ corresponding to turnover rates of 0.056 and 0.034 s^{-1}, respectively.

The interaction of Cy3-EDA-ADP with myosin is a key element in our single-molecule analysis (see below), so the reaction kinetics of Cy3-EDA-ADP (mixed isomers) with subfragment 1 were measured in some detail. Displacement of, typically, 1 μM Cy3-EDA-ADP from 2.5 μM subfragment 1 by 100 μM ATP under the same conditions as in Fig. 2 was accompanied by a decrease in Cy3 fluorescence; the exponential decay was independent of ATP concentration and had a rate constant, k_{+4}, equal to 1.20 ($\pm$ 0.09) s^{-1}. Conversely, the association occurred with an increase in Cy3 fluorescence, and under the same conditions the observed rate constant, k_{obs}, increased linearly with Cy3-EDA-ADP concentration (2.5 to 7.5 μM and 0.5 μM subfragment 1). k_{obs} can be equated with k_{-4}[Cy3-EDA-ADP] + k_{+4}. From these data k_{-4} was 0.53 μM^{-1} s^{-1}, k_{+4} was 1.3 s^{-1}, and the dissociation constant of Cy3-EDA-ADP from subfragment 1, K_4, was 2.6 μM. Further studies were carried out to measure the Cy3-EDA-ADP dissociation rate constant from subfragment 1 over the same temperature range as in the single-molecule studies. At 5 and 10°C, values of k_{+4} were 0.07 ($\pm$ <0.01) and 0.22 ($\pm$ 0.01) s^{-1}, respectively.

The separated isomers 2′-*O*-Cy3-EDA-ATP (and ADP) and 3′-*O*-Cy3-EDA-ATP (and ADP) were isolated in sufficient quantities for their interaction with subfragment 1 to be analyzed. Surprisingly, the fluorescence of 2′-*O*-Cy3-EDA-ATP decreased on binding to subfragment 1, while that of 3′-*O*-Cy3-EDA-ATP increased (Fig. 3, *A* and *B*). From such data, binding of 0.25 μM 3′-*O*-Cy3-EDA-ATP to subfragment 1 was measured over a 1–8-μM range of subfragment 1, and k_{+1} equaled 1.1 $\times$ 10^6 M^{-1} s^{-1} (Table 1). Records as shown in the slow phases in Fig. 3, *C* and *D*, were used to calculate k_{+3} values for 2′-*O*-Cy3-EDA-ATP and 3′-*O*-Cy3-EDA-ATP, respectively, which are recorded in Table 1. The dissociation rate constants of 2′-*O*- and 3′-*O*-Cy3-EDA-ADP were 2.6 and 1.7 s^{-1}, respectively (Fig. 3, *E* and *F*).

Taken together with the K_d (= K_4) value of 2.6 μM (Table 1) for the Cy3-EDA-ADP interaction with subfragment 1, the amplitudes of the records (Fig. 3) show that the fluorescence decrease when 2′-*O*-Cy3-EDA-ADP binds to subfragment 1 is 5% compared to 12% for 2′-*O*-Cy3-EDA-ATP, while the fluorescence increase for 3′-*O*-Cy3-EDA-ADP is 26% compared to 70% for 3′-*O*-Cy3-EDA-ATP. Cutoff filters were used to obtain these data, and it is useful to be able to relate relative fluorescence intensities to a specific emission wavelength. The 70% increase observed when 3′-*O*-Cy3-EDA-ATP binds to subfragment 1 (Fig. 3 *B*) may be compared to the 80% increase for the formation of 3′-*O*-Cy3-EDA-ATP subfragment 1 steady-state complex recorded in an SLM fluorimeter at the maximum emission of 562 nm.

Because Cy5 nucleotides gave a relatively small fluorescence change on interaction with subfragment 1, an indirect fluorescence approach was used to measure the transient kinetics. Mant-ATP was mixed with a solution containing Cy5-EDA-ADP and subfragment 1 at equilibrium (Fig. 4 *A*), and mant-ATP fluorescence was excited by energy transfer from excited tryptophans in subfragment 1. A biphasic increase in fluorescence was recorded. In the absence of Cy5-EDA-ADP, a monophasic fluorescence increase occurred (Fig. 4 *B*), the rate constant of which equaled that of the rapid phase in Fig. 4 *A* and the amplitude of which corresponded to the overall amplitude in Fig. 4 *A*. On the other hand, if the Cy5-EDA-ADP concentration was increased, the ratio of slow to fast phases also increased. The slow phase in Fig. 4 *A* may be equated to the dissociation rate constant, k_{+4}, of 1.6 s^{-1} of Cy5-EDA-ADP from subfragment 1, and the fast phase may be equated to the association of mant-ATP with free subfragment 1 (the process observed in Fig. 4 *B*). The 1:2 ratio of amplitudes of the slow to fast phases gives the ratio between subfragment 1 with Cy5-EDA-ADP bound and free subfragment 1 before mixing in the stopped-flow apparatus. From this the dissociation constant, K_4, can be calculated to be 2.4 μM.

Steady-state kinetic methods were used to measure Michaelis-Menten constants, K'_m for actin and V_{max} of the actin-activated subfragment 1 Cy3-EDA-ATPase and Cy5-EDA-ATPase. However, Cy3-EDA-ATP and Cy5-EDA-ATP were not available at saturating concentrations. Nevertheless, V_{max} values are comparable to those obtained with saturating ATP, although K'_m for actin is two- to threefold greater for the Cy3- and Cy5-nucleotides (Table 1). HPLC records showed that the ratio of isomers of Cy3-EDA-ADP and Cy5-EDA-ADP was unchanged through the time course of the actin-activated triphosphatase assay, indicating that pairs of isomers hydrolyzed at the same rates (within a factor of 1.5; this assay of relative triphosphatase rates has low sensitivity). Transient kinetic methods were used to measure the rates of dissociation of actosubfragment 1 induced by Cy3-EDA-ATP and Cy5-EDA-ATP (Fig. 5 and

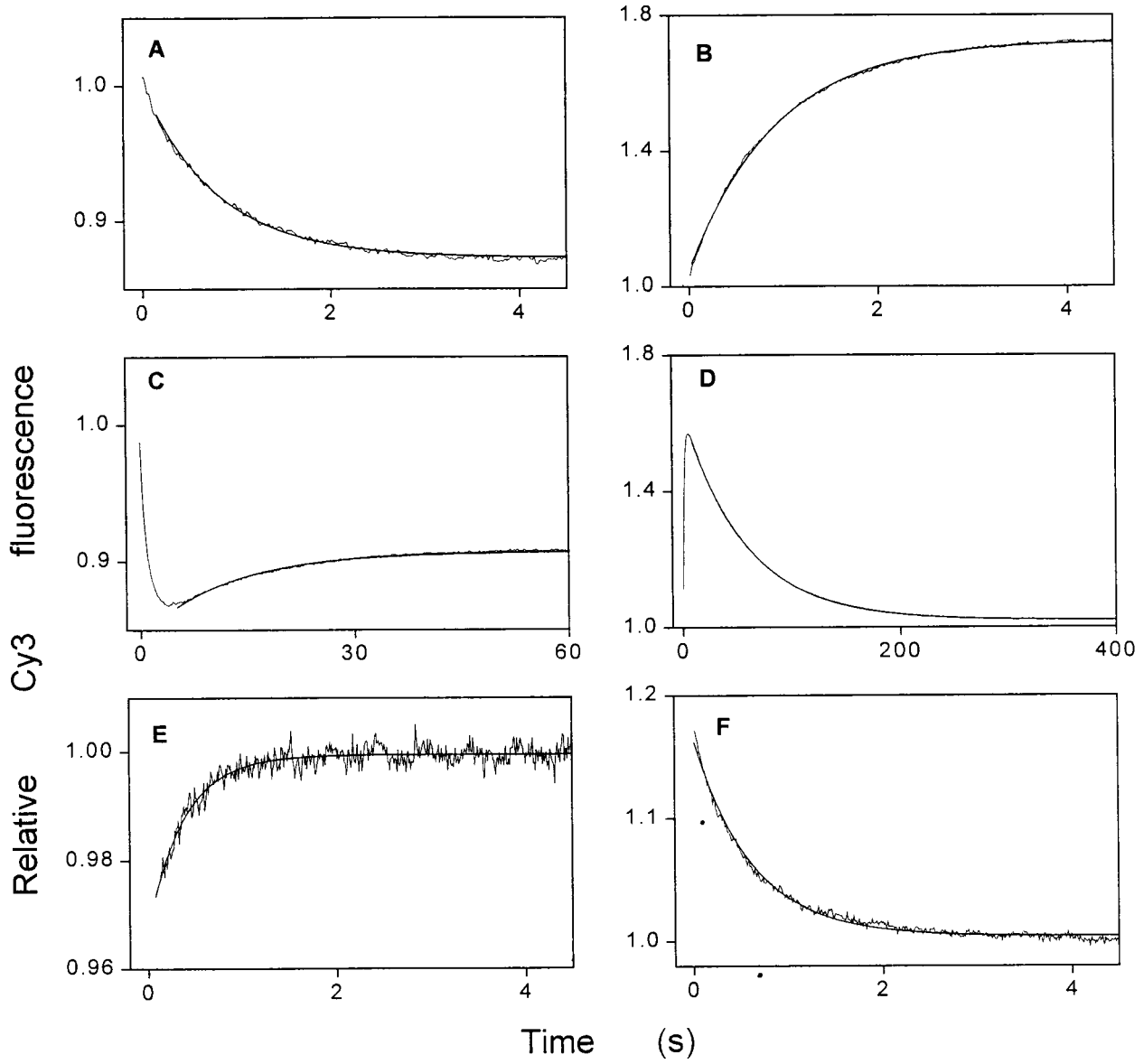

FIGURE 3 Interaction of 2′-*O*- and 3′-*O*-Cy3-EDA-ATP (ADP) with subfragment 1. (*A*) 0.5 μM 2′-*O*-Cy3-EDA-ATP was mixed with 5 μM subfragment 1, and the Cy3 fluorescence change was recorded. (*B*) As in *A* but with 0.5 μM 3′-*O*-Cy3-EDA-ATP. (*C*) As in *A*, with an extended time scale. (*D*) As in *B*, with an extended time scale. (*E*) 50 μM ATP was mixed with 0.77 μM 2′-*O*-Cy3-EDA-ADP and 2.5 μM subfragment 1 (1.53 μM and 5.0 μM, respectively, before mixing). (*F*) As in *E* but with 0.40 μM 3′-*O*-Cy3-EDA-ADP (0.80 μM before mixing) instead of the 2′ isomer. Nonlinear least-squares fits of single exponentials are drawn through the data with rate constants of (*A*) 1.26 s^{-1}, (*B*) 1.15[1], (*C*) 0.085 s^{-1}, (*D*) 0.0185 s^{-1}, (*E*) 2.6 s^{-1}, and (*F*) 1.7 s^{-1}. Reaction conditions were as in Fig. 2.

Table 1). Second-order rate constants were threefold less than for dissociation induced by mant-ATP or ATP.

To compare the kinetics of the Cy3(Cy5)-EDA-nucleotides interacting with subfragment 1 and the kinetics of their interactions with myosin filaments, we needed to measure k_{cat} and k_{+4} in the same solutions. Experiments were carried out in the appropriate solvent (solvent B, Table 2), but using 1 mM rather than 10 mM DTT. The results are recorded in Table 2. k_{cat} values in solvent B were typically twofold greater than those in solvent A (cf. columns 1 and 2 in Table 2). Measurements in other buffer systems showed that this was due primarily to the lower ionic strength of solvent B compared to that of solvent A.

Cy3- and Cy5-EDA-ATP as physiological substrates for muscle fiber contraction

Cy3-EDA-ATP and Cy5-EDA-ATP were compared with ATP as substrates in single permeabilized muscle fibers.

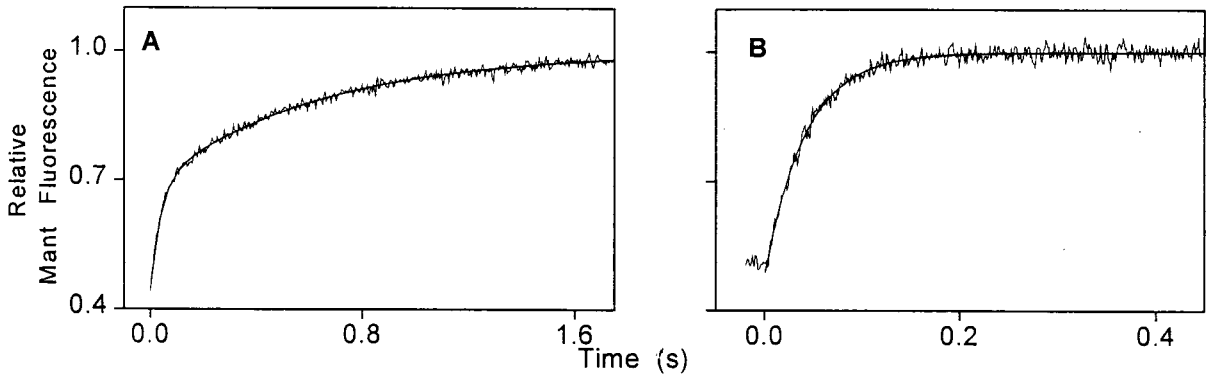

FIGURE 4 Displacement of Cy5-EDA-ADP from subfragment 1. (*A*) 1 μM subfragment 1 and 2 μM Cy5-EDA-ADP (obtained by incubating 2 μM Cy5-EDA-ATP with subfragment 1 for 5 min) mixed with 10 μM mant-ATP. (*B*) As in *A* without Cy5-EDA-ADP. Reaction conditions were as in Fig. 2. Mant-ATP fluorescence was recorded at 430 nm (bandpass filter). In record *B* the fluorescence before time zero arises from mant-ATP during flow. The nonlinear least-squares fit in *A* was to two exponentials with rate constants of 24.9 s^{-1} and 1.6 s^{-1} (relative amplitude 45:55), and the fit in *B* was to a single exponential with a rate constant of 23.9 s^{-1}.

Each analog generated the same isometric force in muscle as ATP. Cy3(Cy5)-EDA-ATP relaxed muscle fibers from the activated state but at a rate fivefold slower than that obtained with the same concentration of ATP. The data from the two assays were very similar to those of a ribose-modified spin-labeled ATP analog (figure 2 of Alessi et al., 1992). The half-times of activation from the relaxed state by Ca^{2+} addition were indistinguishable: between 1.3 and 1.8 s for 0.5 mM analogs and ATP. However, here rates were limited by Ca^{2+} diffusion (Moisescu, 1976), as illustrated by the half-time for activation being 20 ms after photolysis of caged ATP under otherwise comparable conditions (Ellis-Davies and Kaplan, 1994).

The maximum unloaded shortening velocities were 0.63 and 1.31 muscle lengths s^{-1} at 100 μM Cy5-EDA-ATP and ATP, respectively, and 1.73 muscle lengths s^{-1} in 6.25 mM Cy3-EDA-ATP compared to 2.93 muscle lengths s^{-1} in 5 mM ATP (Fig. 6). Thus Cy3- and Cy5-EDA-ATP induce unloaded shortening velocities about twofold more slowly than those achieved with ATP, and this, together with the results of force measurements, shows that they have physiological properties similar to those of ATP.

In vitro motility assay of Cy5-EDA-ATP

The in vitro motility assay was restricted to studies with Cy5-EDA-ATP as a substrate for movement of actin filaments on myosin as the fluorescence of Cy3-EDA-ATP masked that of the rhodamine-phalloidin used to visualize actin filaments. Comparison of in vitro motility induced by Cy5-EDA-ATP was made with mant-ATP rather than ATP. This is because the assay with Cy5-EDA-ATP was restricted to nucleotide analog concentrations less than 3 μM (because of the Cy5 fluorescence masking that of the rhodamine-phalloidin), and at less than 3 μM ATP, no motility was seen (a result also found by Harada et al., 1987).

In the presence of 1 μM Cy5-EDA-ATP, most actin filaments were observed to move slowly and smoothly on a heavy meromyosin-coated glass surface, while no movement was seen below 0.5 μM Cy5-EDA-ATP. There was no obvious difference in the actin movement between that produced in the presence of Cy5-EDA-ATP and that produced with mant-ATP. Little fragmentation of F-actin was observed. The velocities of actin filaments at 0.5, 1, and 2.5 μM Cy5-EDA-ATP were 0.089 ($\pm$ 0.03), 0.21 ($\pm$ 0.05), and 0.43 ($\pm$ 0.13) μm s^{-1}, respectively. These rates are about double those at comparable concentrations of mant-ATP (Fig. 7).

Summary of biochemical and physiological data

These results show that Cy3-EDA-ATP and Cy5-EDA-ATP are good analogs of ATP for the myosin and actomyosin subfragment 1 ATPase in solution, in relaxation and contraction of muscle fibers and in in vitro motility assays. Their diphosphates are good analogs of ADP in its interaction with myosin subfragment 1. These Cy3- and Cy5-nucleotides are therefore suitable candidates for use in studies of the myosin and actomyosin ATPase at the level of single molecules.

The rates of photobleaching of Cy3.29 and Cy5.29 conjugated with myosin

We now turn to results from TIRF microscopy. First photobleaching rates of Cy3.29 and Cy5.29 covalently attached to myosin were determined under the same conditions as for

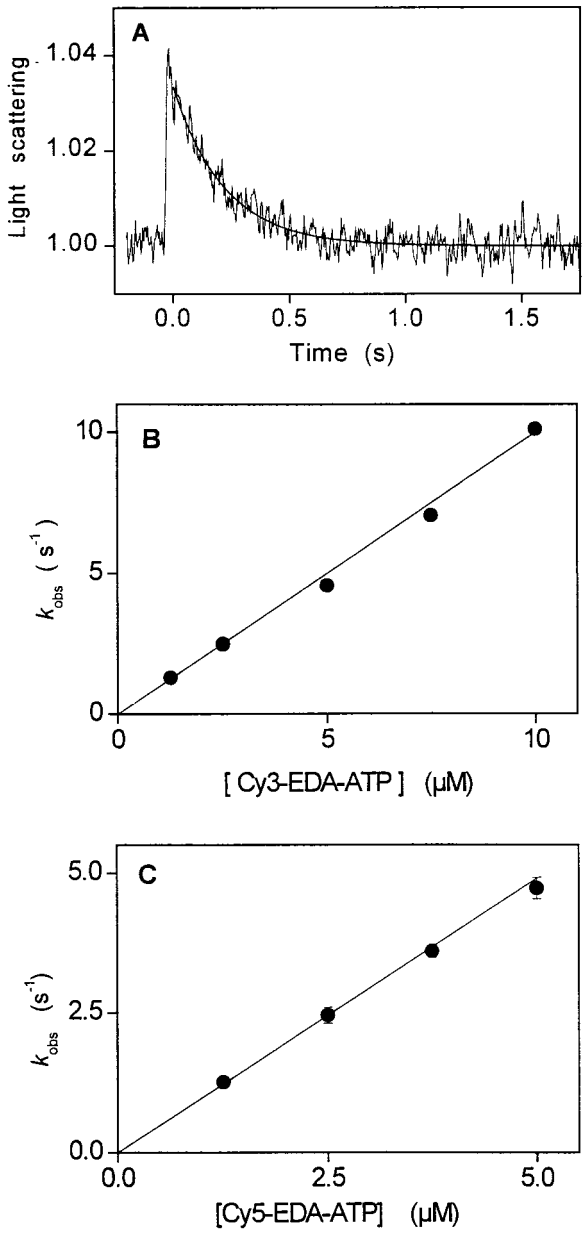

FIGURE 5 Dissociation of actosubfragment 1 induced by Cy3-EDA-ATP and Cy5-EDA-ATP. (*A*) Stopped-flow record of the light scattering change at 350 nm when 0.25 μM subfragment 1 and 0.37 μM actin (reaction chamber concentrations) were mixed with 5 μM Cy5-EDA-ATP. Solution conditions were as in Fig. 2. The solid line is a nonlinear least-squares single exponential fit to the data and has a rate constant, k_{obs}, of 4.76 s^{-1}. The light scattering before zero time is that of the end of the reaction of the previous experimental trial. (*B* and *C*) Concentration dependence of k_{obs} on Cy3-EDA-ATP and Cy5-EDA-ATP. The slope of the least-squares fit to the data (where the solid lines are constrained to pass through the origin) is 0.95 μM^{-1} s^{-1} in *B* and 0.93 μM^{-1} s^{-1} in *C*. SD are shown, except where the deviation was less than the radius of the symbol.

single-molecule observations with the TIRF microscope. The time course of the photobleaching could be fitted by a single exponential decay. For Cy3.29-myosin filaments the rate constant of photobleaching was proportional to the intensity of incident laser power (5–28 mW range); the proportionality factor was 1.5×10^{-4} s^{-1} $(mW)^{-1}$. At an angle of incidence of 70°, the intensity of the evanescent wave within 40 nm (the diameter of a myosin filament) of the surface is three times greater than that of the incident laser (Axelrod et al., 1984). Hence power densities (PDs) averaged over the elliptical Gaussian spot (area 1.3×10^{-8} m^2) include this factor of 3. Thus even at 25 mW (PD = 5.8×10^6 W m^{-2}) the rate of photobleaching of Cy3.29-myosin filaments was only 0.004 s^{-1}. In the case of Cy5.29-myosin filaments, the rates of the photobleaching at 2.4 mW (PD 5.5×10^5 W m^{-2}) and 9 mW (PD 2.1×10^6 W m^{-2}) were less than 0.010 s^{-1} and 0.073 s^{-1}, respectively, the latter rate being comparable to that found by Funatsu et al. (1995).

As described below, single molecules of Cy3-EDA-ATP were routinely seen distinctly and were measured at a laser power of 2 mW at 532 nm, corresponding to an evanescent wave PD averaged over the 6×10^{-9} m^2 elliptical spot of 10^6 W m^{-2}. Because the PD at the peak of the Gaussian spot is twice the average, the maximum PD was 2×10^6 W m^{-2}, and the rate of Cy3 photobleaching was 1.4×10^{-3} s^{-1}, at least an order of magnitude slower than the $1/\tau$ values associated with the interaction between Cy3-EDA-ATP(ADP) and myosin (Table 2). Thus in the single-molecule studies photobleaching did not contribute significantly to the disappearance of individual Cy3-EDA-ATP molecules from myosin filaments. However, photobleaching was less satisfactory for Cy5-EDA-ATP. Thus while we report ensemble data from TIRF microscopy for Cy5-EDA-ATP interacting with myosin filaments, we report single-molecule data only for Cy3-nucleotides.

Macroscopic interactions of Cy3- and Cy5-EDA-nucleotides with immobilized myosin filaments

When perfused with Cy5-EDA-ATP, individual myosin filaments attached to the surface were observed as fluorescent images (Fig. 8 *A*). Myosin filaments were sufficiently firmly attached to the surface that they were not flushed away with perfusion of fresh buffer into the observation chamber. The intensity of the fluorescent images of myosin filaments depended on the concentration of Cy5-EDA-ATP, and it decreased to the same intensity as that of the background fluorescence when an excess of ATP was perfused. These findings suggest that we observed fluorescence solely from Cy5-EDA-ATP binding to myosin molecules at ATP binding sites with no extraneous cyanine dye binding. An attempt was made to measure the K_m of Cy5-EDA-ATP associated with myosin-catalyzed hydrolysis from the fluorescence intensity of individual myosin filaments at various concentrations of Cy5-EDA-ATP. The intensity began to show saturation behavior at 50 nM. Higher concentrations

TABLE 2 Comparison of rate constants measured by stopped flow and TIRF

		Subfragment 1 (stopped flow)		Myosin filament (TIRF)	
Nucleotide	Temperature (°C)	Solvent A* k_{cat} (s^{-1})†	Solvent B* k_{cat} (s^{-1})	Ensemble k_{diss} (s^{-1})	Single molecule $1/\tau$ (s^{-1})
2′(3′)-*O*-Cy3-EDA-ATP	20	0.022 (±0.001 SD)‡	0.042 (±0.003)	0.037 (±0.010)	0.24 (±0.06)
2′-*O*-Cy3-EDA-ATP	20	0.080 (±0.002)	0.1–0.2§	0.10 (±0.03)	0.14¶
3′-*O*-Cy3-EDA-ATP	20	0.022 (±0.001)	0.038 (±0.004)	0.049 (±0.029)	0.12¶
2′(3′)-*O*-Cy5-EDA-ATP	25	0.027 (±0.002)‖	0.060 (±0.006)	0.047 (±0.022)	ND
		k_{+4} (s^{-1})	k_{+4} (s^{-1})	k_{diss} (s^{-1})	$1/\tau$ (s^{-1})
2′(3′)-*O*-Cy3-EDA-ADP	10	0.21 (±0.04)	0.22 (±0.01)	0.58 (±0.22)	0.39 (±0.07)
2′(3′)-*O*-Cy3-EDA-ADP	20	1.20 (±0.09)	1.44 (±0.01)	1.41 (±0.46)	ND

*Solvent A is an aqueous solution of 100 mM KCl, 5 mM $MgCl_2$, 1 mM DTT, and 50 mM Tris adjusted to pH 7.5 with HCl. Solvent B is an aqueous solution of 2 mM $MgCl_2$, 1 mM EGTA, 10 mM DTT, and 20 mM PIPES adjusted to pH 7.8 with KOH.

†k_{cat} and k_{+4}, as in Table 1; k_{diss}, TIRF ensemble displacement rate constant; $1/\tau$, reciprocal of the mean lifetime; SD, standard deviation.

‡SDs measured in stopped-flow experiments are derived from single subfragment 1 preparations. As described in Data Analysis and Curve Fitting, the estimated maximum range of k_{cat} and k_{+4} is 0.7- to 1.4-fold of the quoted value.

§The small signal amplitude only permitted k_{cat} to be measured approximately.

¶Single measurement, hence no SD quoted.

‖The value of k_{cat} at 25°C is less than that at 20°C (Table 1); measurements were made with separate subfragment 1 preparations. However, when k_{cat} was measured at 20°C and 25°C on the same subfragment 1 preparation, the values obtained were 0.022 s^{-1} and 0.034 s^{-1}, respectively (i.e., showing the expected temperature effect).

of Cy5-EDA-ATP could not be used, because of interference from background fluorescence.

To measure the Cy5-EDA-ATPase of myosin filaments, 1 mM ATP was perfused into a flow cell containing 50 nM Cy5-EDA-ATP and myosin filaments to displace the steady-state complex. This is a sufficient concentration of ATP to ensure that in this and subsequent displacement experiments, influx of the ATP is not rate-limiting (see Materials and Methods and Fig. 8 *B, inset*). The Cy5 fluorescence decayed exponentially with a rate constant of 0.047 (± 0.022) s^{-1} ($n = 6$) (Fig. 8 *B*), and this corresponds to the Cy5-EDA-ATPase rate measured with subfragment 1 in solution (solvent B, Table 2).

To examine the effect of actin, myosin filaments were incubated with 300 nM phalloidin-stabilized actin filaments and 50 nM Cy5-EDA-ATP. Myosin filaments were observed as fluorescent images, but in a typical assay the fluorescence intensity was ~60% of that in the absence of actin. This probably reflects a higher K_m of Cy5-EDA-ATP in the presence of actin and, possibly, as considered in the Discussion, a different fluorescence intensity of the actin-activated Cy5-EDA-ATPase steady-state complex. When perfused with 1 mM ATP, the fluorescence of the Cy5-EDA-ATP bound to myosin filaments disappeared in a single exponential decay (Fig. 8 *C*) at 0.12 (± 0.09) s^{-1} ($n = 6$), about a threefold acceleration of the rate in the absence of actin.

Displacement of 50 nM Cy3-EDA-ATP (mixed isomers) from myosin filaments by 1 mM ATP, done in the same fashion as for Cy5-EDA-ATP in Fig. 8 *B*, resulted in a biphasic transient. This is not surprising in view of the distinct 2′- and 3′-*O*-Cy3-EDA-ATPase activities in solution (Table 2). However, even the pure isomers exhibited transient fluorescent decays that did not fit clean single exponentials. We analyzed these records in two ways. First, results are recorded in Table 2 as a best fit to a single exponential decay for ease of comparison with single-molecule and stopped-flow data. Second, records were analyzed as a best fit to two exponentials. For nine 2′-*O*-Cy3-EDA-ATP displacement assays, rate constants for the fast and slow phases were 0.190 (± 0.037) s^{-1} and 0.032 (± 0.009) s^{-1}, respectively, with a ratio of the amplitude of the fast to slow phases of 1.23 (± 0.74). For nine 3′-*O*-Cy3-EDA-ATP displacement assays the corresponding values were 0.084 (± 0.038) s^{-1}, 0.018 (± 0.012) s^{-1}, and 1.37 (± 1.13). There was thus considerable variation in the relative amplitudes of the fast and slow phases for both isomers.

The dissociation rate constant of Cy3-EDA-ADP from myosin filaments was measured and compared with that obtained in the stopped-flow experiments. A sixfold greater concentration of diphosphate over triphosphate was needed because the K_d of Cy3-EDA-ADP and myosin is larger than the K_m of Cy3-EDA-ATP (based on comparison of K_4 and k_{+3}/k_{+1} ($= K_m$) in column 1 of Table 1). Experiments in which Cy3-EDA-ADP was displaced from myosin filaments by ATP were conducted at 10°C as well as at 20°C, so the results could be compared with those of single-molecule studies (see below). Fig. 9 *A* shows qualitatively the exponential decay of Cy3 fluorescence in two myosin filaments as Cy3-EDA-ADP was displaced by ATP, and Fig. 9, *B* and *C*, records rate constants of 0.87 s^{-1} at 10°C and 1.56 s^{-1} at 20°C measured from one of the filaments. The results from several experiments gave 0.58 (± 0.22) s^{-1} ($n = 6$) at 10°C and 1.41 (± 0.46) s^{-1} ($n = 9$) at 20°C.

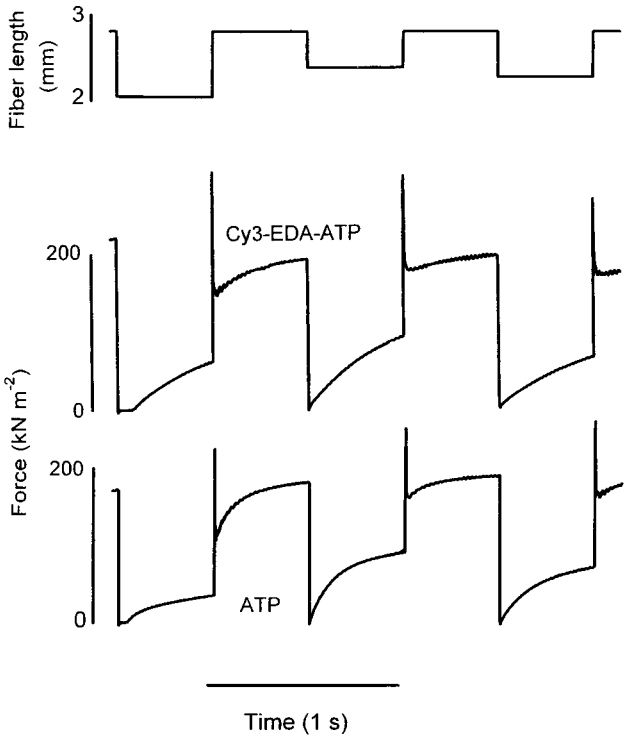

FIGURE 6 Shortening velocity of a rabbit psoas muscle fiber with Cy3-EDA-ATP and ATP. The records are from a slack test performed in 6.25 mM Cy3-EDA-ATP or 5 mM ATP at 20°C and pH 7.1. The sarcomere length was set to 2.6 μm before fiber activation. The lower two records show the force response to length changes shown in the upper record. After the first fiber length decrease from 2.8 to 2 mm, there are delays of 72 ms in the case of Cy3-EDA-ATP and 48 ms in the case of ATP before force begins to increase. With the smaller length decreases the delays are barely discernible and are in the range of 5–20 ms. The decrease in isometric force from 215 kN m^{-2} at the start of the Cy3-EDA-ATP record to 165 kN m^{-2} at the start of the ATP record is ascribed to fiber rundown and not to the isometric force being nucleotide specific.

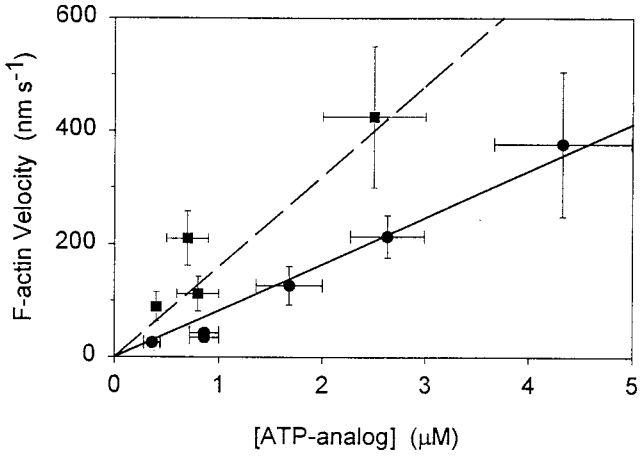

FIGURE 7 Dependence of F-actin velocity on ATP analog concentration in the in vitro motility assay. Velocities of rhodamine-phalloidin-labeled F-actin (10 nM in G-actin) were measured at 25°C on a bed of heavy meromyosin at the Cy5-EDA-ATP (■) or mant-ATP (●) concentrations indicated in the motility buffer (see In Vitro Motility Assay). SD are shown and were necessary for ATP analog concentrations because of the uncertainty in the flow-cell dead volume. The dashed line has a slope of 160 nm s^{-1} μM^{-1}, and the solid line has a slope of 82 nm s^{-1} μM^{-1}. Each is a least-squares fit to the data and is drawn to pass through the origin.

Observations of single Cy3-EDA-ATP molecules on immobilized myosin filaments

Assuming that the K_m of Cy3-EDA-ATP for myosin is ~40 nM (see Discussion), and a 2.6-μm myosin filament contains a thousand myosin heads (see below), we can expect a Poisson distribution with zero, one, or a few discrete fluorescent spots on an individual filament when it is equilibrated with 50 pM Cy3-EDA-ATP.

Typical images of fluorescent spots observed on a myosin filament and the time course of the corresponding fluorescence intensity of the myosin filament are shown in Fig. 10. The spot abruptly appeared on a myosin filament, stayed at the same position for a while, and then disappeared abruptly. Although the intensity and the size of these spots fluctuated, they were clearly distinct from the background fluorescence, and single spots observed at their peak intensities had a mean diameter of e^{-1} times their peak intensity of less than 1 μm. To confirm that these spots are on myosin filaments, the positions of myosin filaments were identified as fluorescent images by perfusion of 2–10 nM Cy3-EDA-ATP at the beginning and 50 nM at the end of the observation (L in Fig. 10). Thus the discrete turning on and off of a fluorescent spot was interpreted to show binding and detachment (after hydrolysis) of a Cy3-EDA-ATP molecule on a myosin head, although artifact spots with a long dwell time were occasionally observed in the absence of Cy3-EDA-ATP. At the laser PD used, there was no evidence of reversible photobleaching events such as "blinking" (Dickson et al., 1997; Xie and Trautman, 1998; M. Kikumoto, K. Oiwa and M. Anson, unpublished data).

Under the above conditions an emission rate from individual Cy3-EDA-ATP molecules of 10^5 photons s^{-1} is expected (Anson and Oiwa, 1998), with ~1% of these being detected and imaged. When analyzed as a shot-noise limited process (Rice, 1954), this gives a signal-to-noise ratio of 16 averaged over 0.27 s (eight video frames), as was observed qualitatively (Fig. 10).

If two or more molecules occupied the same region of a myosin filament to generate an apparent single spot, then quantal levels of intensity might be expected to occur during the lifetime of such spots. This effect was seen occasionally, but variations in spot intensity precluded quantitative analysis. However, there was a linear relation between the intensity and its variance, as predicted for a process obeying Poisson statistics (Rice, 1954). In practice the vast majority of spots just switched on and off, suggesting that, in general, a fluorescent spot reflects a single nucleotide molecule binding to the filament.

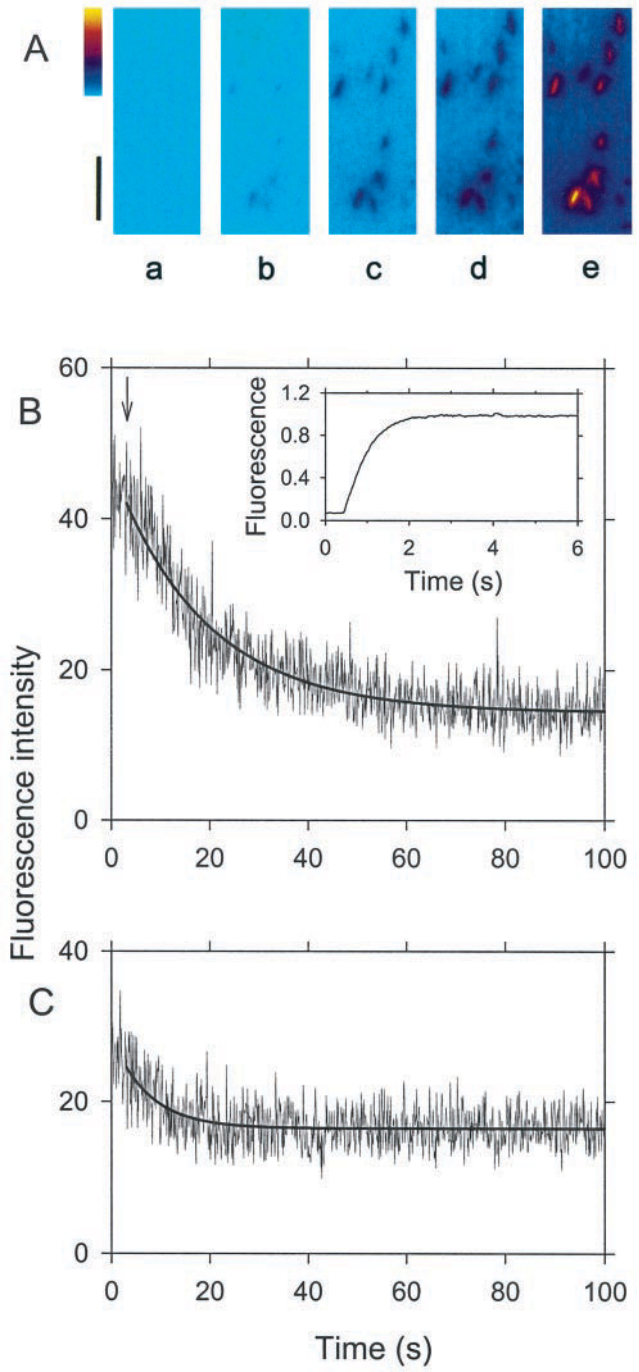

FIGURE 8 Fluorescence intensity of Cy5-EDA-ATP interacting with immobilized filaments in solvent B at 25°C. (*A*) Pseudocolor displays of fluorescence images of myosin filaments visualized with the perfusion of various concentrations of Cy5-EDA-ATP were obtained in identical fields of view by accumulating 256 successive video frames and digitizing with a video image processor. The concentrations of Cy5-EDA-ATP were zero in *a*, 1 nM in *b*, 2 nM in *c*, 5 nM in *d*, and 10 nM in *e*. A scale bar of 5 μm and a linear 0–255 pseudocolor scale of fluorescence intensity are shown. (*B*) The filament was first incubated in 50 nM Cy5-EDA-ATP. Then 1 mM ATP in the same solution (including 50 nM Cy5-EDA-ATP) was rapidly exchanged into the field of view. (*C*) As in *B*, except that phalloidin-stabilized F-actin (300 nM in G-actin) was present before and after ATP addition. The solid lines are single exponential nonlinear least-squares fits to the data with endpoints at 12 and 16 fluorescence intensity and rate constants of 0.04 s^{-1} and 0.14 s^{-1} in *B* and *C*, respectively. The inset in *B* shows the rate of Cy5 fluorescence change when Cy5.29.OH was perfused into the observation cell (see Materials and Methods).

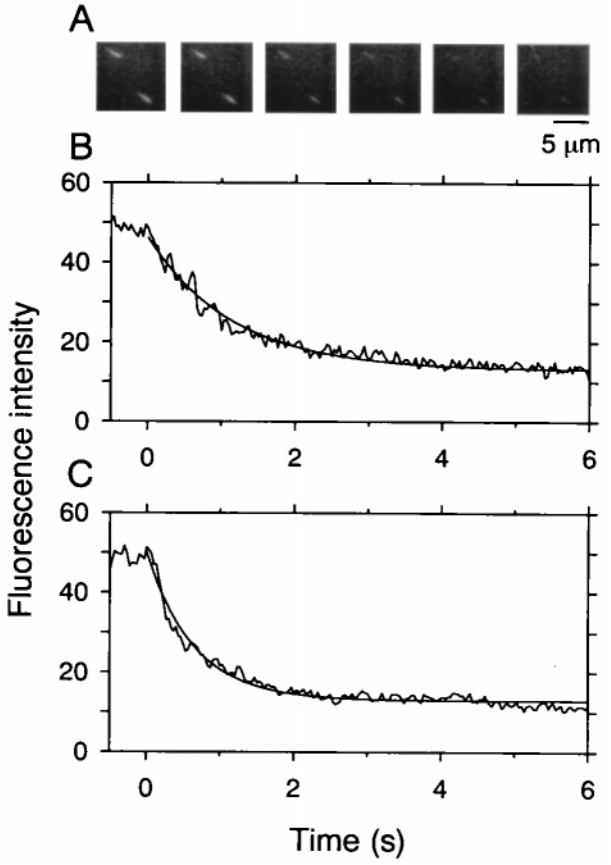

FIGURE 9 Cy3-fluorescence change of an immobilized myosin filament after Cy3-EDA-ADP displacement by ATP. (*A*) A succession of 33-ms frames recorded at 330-ms intervals, showing the fluorescence decay (arbitrary scale) when two myosin filaments incubated at 10°C in 300 nM Cy3-EDA-ADP were treated with 1.6 mM ATP that was rapidly exchanged into the field of view. (*B*) Time record of the Cy3 fluorescence from the upper left myosin filament from 1 s before ATP washout. (*C*) As in *B* but at 20°C. The solid lines are single-exponential nonlinear least-squares fits to the data with rate constants of 0.87 s^{-1} and 1.56 s^{-1} in *B* and *C*, respectively.

It is important to be able to carry out single-molecule experiments in which all or most myosin sites contain bound nucleoside triphosphate, for example, when single molecules on myosin are observed in the presence of moving actin filaments (i.e., avoiding the rigor state). This requires a mixture of fluorescent and nonfluorescent triphosphate to minimize background fluorescence and to ensure that a spot arises from only one or a few fluorophores. Using the same protocol as in Fig. 10 but in the presence of 10 nM Cy3-EDA-ATP and 10 μM ATP, discrete fluorescent spots were observed on myosin filaments because the 1000-fold excess of ATP over Cy3-

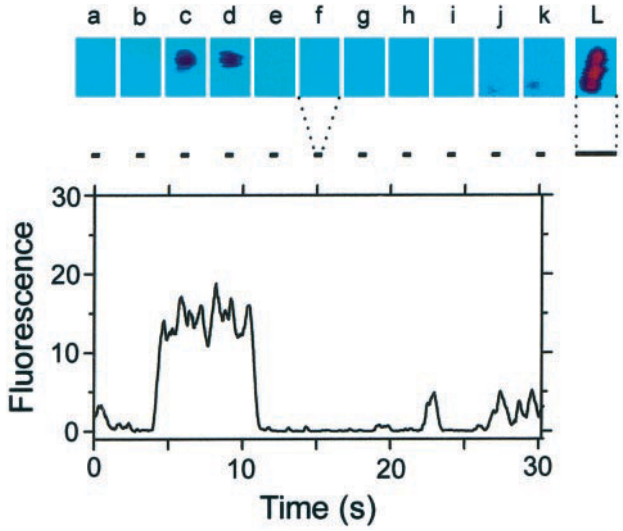

FIGURE 10 Pseudocolor display of single-molecule events deduced from Cy3-fluorescence when 50 pM Cy3-EDA-ATP interacts with a myosin filament. The microscopic field was illuminated with 7.0 mW (3.5×10^6 W m^{-2}) laser power at 514.5 nm. Images *a–k* and *L* have dimensions of 7×10 μm and a linear 0–255 pseudocolor scale of fluorescence intensity. Images *a–k* were recorded over 0.27 s (eight video frames rolling-averaged), as indicated by the short bars at 3-s intervals. Image *L* was recorded over 3 s from the filament bathed in 50 nM Cy3-EDA-ATP. The line trace is the time course of fluorescence intensity (arbitrary scale) integrated over the 7×10 μm observation area. A zero fluorescence cutoff was set by the background from an area without filaments. The "blips" (e.g., at ~23 s) were caused by thermal noise in the detector, and their presence is also just evident in images *j* and *k*.

EDA-ATP also ensured a distribution of zero, one, or a few discrete spots per filament.

We then checked whether the observed pattern and frequency of fluorescent spots was consistent with Michaelis-Menten behavior. The K_m of an ATP analog for myosin permits an estimate of the distribution of number frequency of nucleotide molecules bound to a filament. Taking K_m for Cy3-EDA-ATP to be 40 nM (see Discussion), the ratio between myosin heads having Cy3-EDA-ATP bound and free heads is 1:800 at a concentration of 50 pM Cy3-EDA-ATP. The bipolar myosin filaments have a mean length of 2.6 μm. After correcting for the 0.16-μm bare zone (Craig, 1977), the number of myosin molecules in the three-strand filament (Kensler and Stewart, 1993) was calculated to be 500. Hence it follows that the average number of Cy3-EDA-ATP molecules bound to a filament is 1.25. The Poisson distribution predicts probabilities of 0.29, 0.36, 0.22, and 0.13 of finding zero, one, two, or more molecules bound to a single filament. When the frequency of occurrence was plotted against the observed intensity (data not shown), the data, though noisy, were consistent with this model.

A montage of fluorescent spots derived from single molecules of Cy3-EDA-ATP interacting with myosin filaments is shown in Fig. 11. The kinetics of the interaction were established from the dwell times (Fig. 12 *A*). From the exponential fit to the distribution, the reciprocal of the mean lifetime, $1/\tau$, of fluorescent spots was 0.14 s^{-1}. In contrast, the dwell time of the spots became shorter when 300 nM phalloidin-stabilized actin was added to myosin filaments (Fig. 12 *B*), and $1/\tau$ equaled 0.33 s^{-1}. Averaged over all data, $1/\tau$ was 0.24 ($\pm$ 0.06) s^{-1} in the absence of actin and 0.78 ($\pm$ 0.34) s^{-1} in the presence of 600 nM actin.

The $1/\tau$ values of the separated 2′- and 3′-*O*-Cy3-EDA-ATP on myosin filaments differed by a factor of 1.2, threefold less than the difference in the Cy3-EDA-ATPase of the two isomers in solution (Fig. 13 and Table 2). It was not possible to distinguish the intensity of fluorescent signals of 2′- and 3′-*O*-Cy3-EDA-ATP bound to myosin filaments, despite the fact that the absolute fluorescence of the 2′ isomer bound to subfragment 1 is 0.6 that of the bound 3′ isomer. This is not surprising, in view of the dependence of the intensity of the evanescent wave on its distance from the silica-water interface.

Dissociation rate of single Cy3-EDA-ADP molecules from a myosin filament

The interaction of single Cy3-EDA-ADP molecules with a myosin filament was studied. Because the K_d of Cy3-EDA-ADP from myosin is ~3 μM, and, using the same argument as above for optimal observation of single molecules of Cy3-EDA-ATP, a Poisson distribution with zero, one, or a few discrete fluorescent spots was expected on an individual filament when it was equilibrated with 3 nM Cy3-EDA-ADP.

It was difficult to measure the dwell times of single molecules of Cy3-EDA-ADP on myosin filaments at 20°C because they were comparable to the 270-ms time resolution of the technique. Furthermore, the 60-fold higher concentration of Cy3-EDA-ADP compared with Cy3-EDA-ATP caused greater background fluorescence. Nevertheless it was possible to measure the dwell times associated with Cy3-EDA-ADP over the temperature range 5–10°C after first locating the filaments with 300 nM Cy3-EDA-ADP (as in Fig. 9 *A*). The distributions of dwell times shown in Fig. 14 were exponential with fitted $1/\tau$ values of 0.18, 0.22, and 0.435 s^{-1} at 5, 7, and 10°C, respectively. Thus measurement of the kinetics of Cy3-EDA-ADP dissociation from myosin subfragment 1 or myosin filaments afforded a second comparison of ensemble and single-molecule kinetics (Table 2).

DISCUSSION

The principal aim of the present study is to establish a reliable framework within which single-molecule enzymology can be undertaken, using the hydrolysis and reversible binding of fluorescent ATP analogs interacting with myosin as a model system. Myosin has the experimental advantage that it forms filaments that are easily located. Previous experience has shown that modification of the 2′- or 3′-

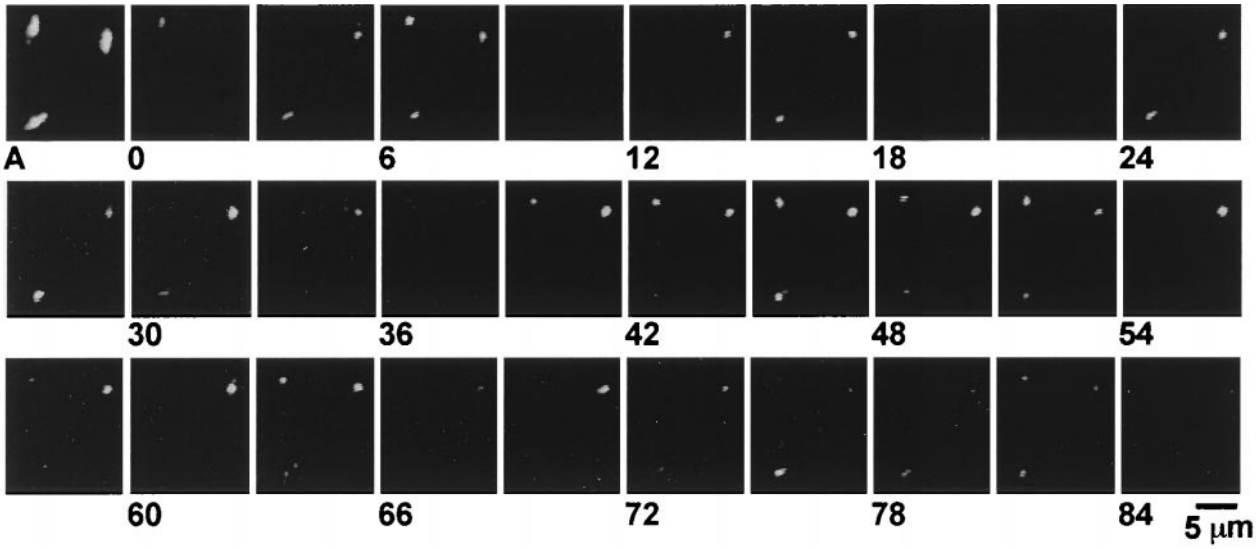

FIGURE 11 Time sequence of single molecules of Cy3-EDA-ATP binding to three myosin filaments. The first frame (*A*) shows the positions of the three synthetic myosin filaments after perfusion with 2 nM Cy3-EDA-ATP. After the nucleotide was washed out, 50 pM Cy3-EDA-ATP was infused, and single molecules can be seen binding to the filaments. Illumination conditions were as in Fig. 10. Each photograph represents a running average of 32 video frames (1.1 s) with contrast enhancement. Numbers under the frames indicate the time (s) when the image was obtained. A 5-μm scale bar is shown.

ribose hydroxyl groups leads to ATP analogs that are excellent substrates for myosin and actomyosin and that support muscle contraction. This, together with the fluorescent properties of cyanine dyes, made 2′- and 3′-cyanine-substituted ATP derivatives the analogs of choice. However, it is preferable to work with one nucleotide rather than a mixture of fluorescent nucleotides. For this reason we have separated 2′- and 3′-*O*-Cy3-EDA-ATP(ADP), studied the kinetics of their interconversion, and established conditions under which isomerization can be avoided.

General properties of ribose-modified nucleotides and cyanine dyes

Carbamoyl esters are more resistant to hydrolysis than simple esters; therefore the isomers of 2′- and 3′-carbamoyl

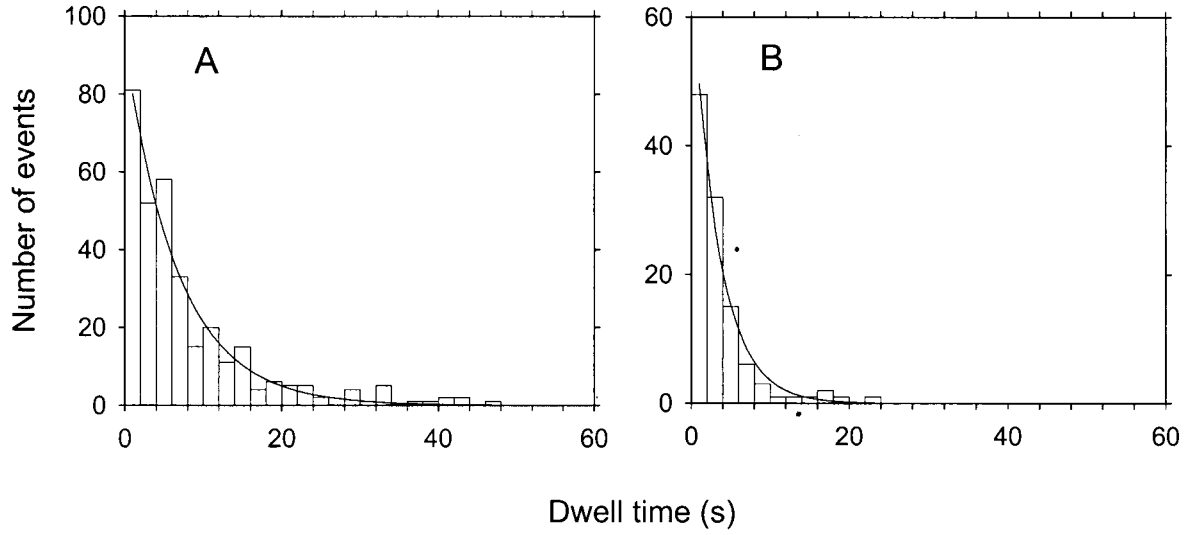

FIGURE 12 Distributions of dwell times of fluorescent spots observed on myosin filaments in solvent B plus the oxygen depletion reagents in the presence of 50 pM Cy3-EDA-ATP. All observations longer than 1 s were fitted by the nonlinear least-squares method with an exponential distribution; zero time on the abscissa is at the end of this 1 s. (*A*) In the absence of F-actin, the histogram of dwell times was fitted with a single exponential decay of reciprocal mean lifetime $1/\tau$, equal to 0.14 s^{-1}. (*B*) In the presence of 300 nM F-actin, the histogram was fitted by $1/\tau$ equal to 0.33 s^{-1}.

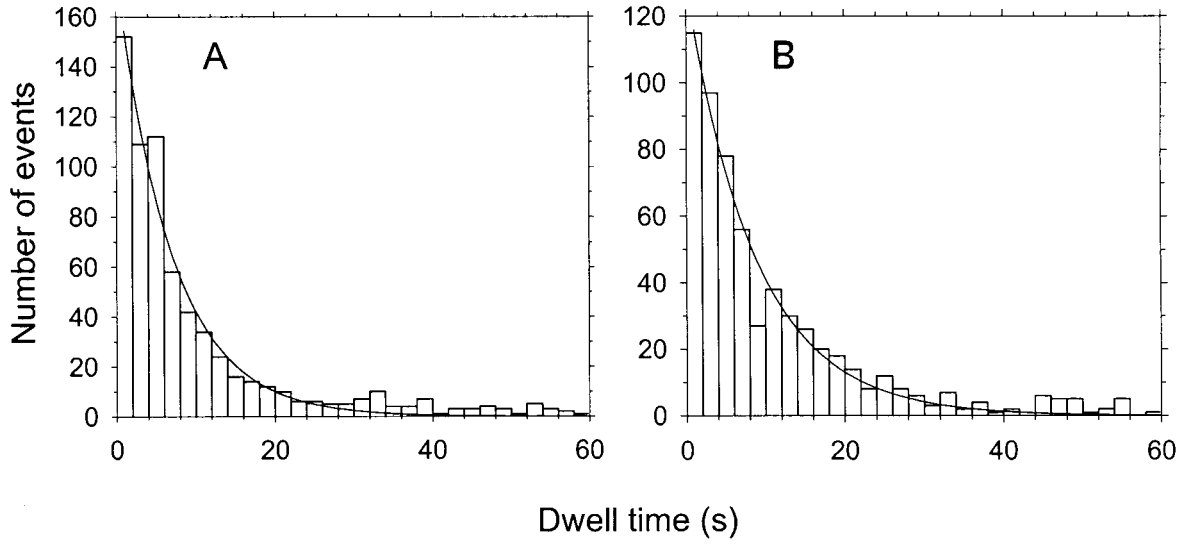

FIGURE 13 Distribution of dwell times of fluorescent spots as in Fig. 12, observed on myosin filaments in the presence of separated isomers of Cy3-EDA-ATP. Histograms from (*A*) 50 pM 2′-*O*-Cy3-EDA-ATP and (*B*) 50 pM 3′-*O*-Cy3-EDA-ATP were fitted with $1/\tau$ of 0.14 s^{-1} and 0.115 s^{-1}, respectively.

esters were likely to isomerize more slowly than 2′(3′)-*O*-carboxy esters and so be more readily separable. Separation was first established with 2′- and 3′-*O*-Ac-EDA-ADP, because these compounds were more readily available than their cyanine counterparts. As expected, the isomerization rate of 2′(3′)-*O*-ribose-substituted carbamoyl esters was about three orders of magnitude slower than the isomerization rate of the 2′(3′)-*O*-carboxylate esters of mant-ATP. Isomerization rates for other esters will vary, depending, for example, on the pK_a or stereochemistry of the carbamic or carboxylic acid (Griffin et al., 1966). The importance of the slow isomerization rate was borne out in the separation of 2′- and 3′-*O*-Cy3-EDA-ATP. Aqueous solutions of TEAB form alkaline solutions of pH ~10 during evaporation of the salt in vacuo (data not shown), and alkalinity promotes isomerization. However, using rapid evaporation, 10-nmol quantities of 2′- and 3′-*O*-Cy3-EDA-ATP were concentrated from TEAB buffer with minimal isomerization. The slow isomer-

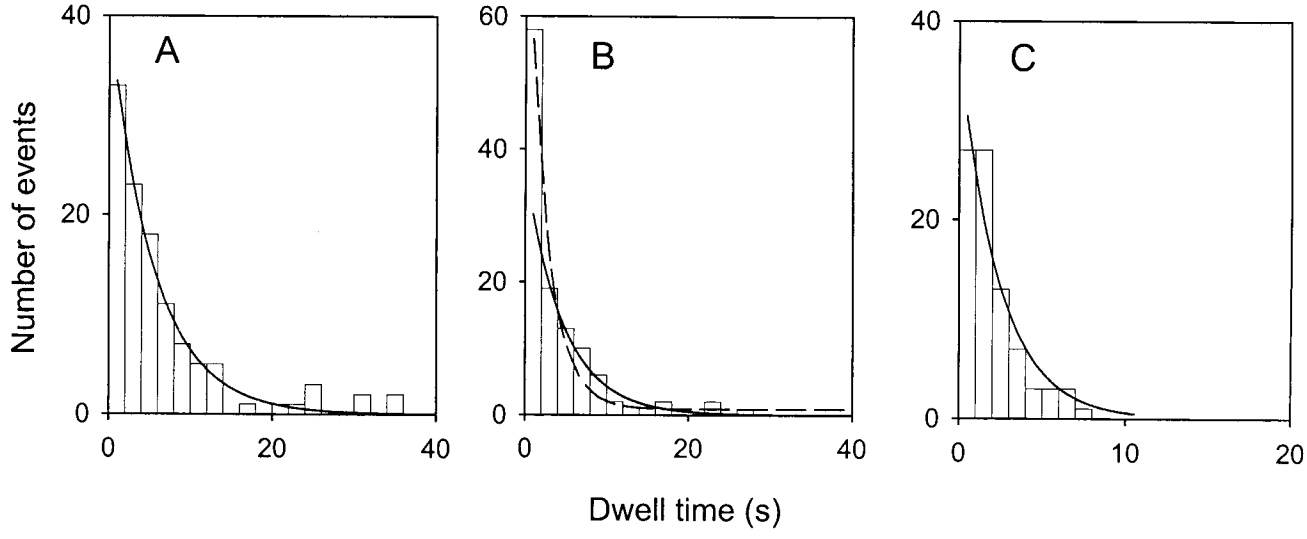

FIGURE 14 Distributions of dwell times of fluorescent spots as in Fig. 12, observed on myosin filaments in the presence of 3 nM Cy3-EDA-ADP. Histograms measured at (*A*) 5, (*B*) 7, and (*C*) 10°C were fitted with $1/\tau$ of 0.18 s^{-1}, 0.22 s^{-1}, and 0.435 s^{-1}, respectively. In *B* the number of events in the 0–2-s bin appears anomalously high, and this bin is omitted from the solid-line fit ($1/\tau$ 0.22 s^{-1}). The dashed line in *B* is the fit if the 0–2-s bin is included ($1/\tau$ 0.37 s^{-1}).

ization rate of the carbamoyl esters also means that it is practical to carry out relatively long biological experiments with one or another isomer. We found no evidence of subfragment 1-promoted isomerization, a result similar to that found by Cheng et al. (1998) with 2′(3′)-*O*-mant-ADP.

The extinction coefficients, ϵ, of the cyanine dyes are worthy of comment because of their magnitude. It is important to check whether these high ϵ values provide evidence for intermolecular interactions, which might produce anomalies when single-molecule events of cyanine dyes are compared with ensemble behavior. A measure of the intensity of an electronic transition is the oscillator strength f, a dimensionless quantity that is the sum of all possible electronic transitions and cannot exceed unity for a single electron (Dexter, 1958). f is related to the integral of ϵ (M^{-1} cm^{-1}) over the range of frequency, ν (Hz), of the ground-state absorption band by $f = 1.213 \times 10^{-19} \int \epsilon \, d\nu$, where the numerical constant takes into account the refractive index of water (1.334) and the Lorentz-Lorenz effect of polarizability (Born and Wolf, 1997; Dexter, 1958). $f = 0.89$ for Cy3 from the absorption spectrum of Cy3.29.OH in aqueous solution. $f = 1.02$ for Cy5 from the absorption spectrum of Cy5.29.OH, based on our measured ϵ_{max} of 218,000 M^{-1} cm^{-1}, while $f = 1.17$ for the published ϵ_{max} of 250,000 M^{-1} cm^{-1}. The lower value of 1.02 equals unity within the limits of experimental error consistent with a single electronic transition. Thus there is no evidence for anomalous optical properties in the cyanine dyes.

Cy3- and Cy5-EDA-ATP as substrates for (acto)myosin and muscle contraction

Cy3-EDA-ATP and Cy5-EDA-ATP were substrates for myosin and actomyosin subfragment 1 in solution, with kinetic parameters similar to those for ATP (Table 1). Their K_m values when they were substrates for subfragment 1 can be estimated from $K_m = (k_{cat} + k_{-1})/k_{+1} = k_{cat}/k_{+1}$, presuming that $k_{-1} \ll k_{cat}$, as is probable (Bagshaw and Trentham, 1973; Goody et al., 1977). From the data in Table, 1 K_m values for 2′-*O*-Cy3-EDA-ATP, 3′-*O*-Cy3-EDA-ATP, and 2′(3′)-*O*-Cy5-EDA-ATP are 70, 20, and 25 nM, respectively. It follows that K_m is 40 nM for an equilibrium mixture of 2′(3′)-*O*-Cy3-EDA-ATP from the 70 and 20 nM K_m values of the separated isomers and their equilibrium constant of 1.43.

The analogs were effective physiological substrates in muscle fibers with unloaded shortening velocities that were about half of those produced by ATP. Cy5-EDA-ATP also supported the movement of actin filaments in the in vitro motility assay (Fig. 7). Actin filament velocity was compared with that induced by mant-ATP, for which the saturating velocity, V_o, is 50% that of ATP (data not shown). Though, as noted earlier, filament velocity does not follow simple saturation kinetics as a function of ATP concentration, comparison of the parameter V_o/K_m (70 nm s^{-1} μM^{-1} for ATP; Homsher et al., 1992) is possible. From the slope in Fig. 7, V_o/K_m is 160 nm s^{-1} μM^{-1} for Cy5-EDA-ATP, 2.3-fold greater than for ATP. If we suppose that the maximum unloaded shortening velocities (Fig. 6) are proportional to V_o with the same proportionality constant (1.8 in rat skeletal muscle; Canepari et al., 1999), it follows that the K_m of Cy5-EDA-ATP is ~0.22-fold that of ATP (60 μM) in the motility assay (Harada et al., 1987; Kron and Spudich, 1986). This K_m value is half the 25 μM estimate from the data in Table 1. Overall the kinetic results of cyanine nucleotides interacting with isolated proteins and fibers are consistent with previous observations that show biological function is maintained after ribose modification of ATP (Alessi et al., 1992; Hiratsuka, 1983, 1984; Mahmood et al., 1987; Woodward et al., 1991).

The optical properties of the two fluorophores dictated which one was preferable for use in particular circumstances. The larger fluorescence signal when Cy3-EDA-ATP interacts with subfragment 1 (Fig. 2) makes Cy3 the fluorophore of choice for transient kinetic studies. Cy5-EDA-ATP was preferable in the in vitro motility assay because the Cy3 fluorescence overlapped that of the rhodamine-labeled phalloidin used to detect the actin filaments. On the other hand, Cy3-EDA-ATP could of course be used by labeling actin with a different fluorophore. Cy3 was preferred in single-molecule studies, primarily because of its greater photostability; results reported here are confined to that fluorophore.

Distinctions between 2′- and 3′-*O*-substituted isomers

The similarity or otherwise of the kinetics of 2′- and 3′-substituted isomers of ATP interacting with (acto)myosin at the macroscopic level has an important bearing on the analysis of single-molecule events. The rate constants of the association steps between 2′- and 3′-*O*-Cy3-EDA-ATP isomers and subfragment 1 are indistinguishable (Table 1). However, the rate constant of the slower phase in single-turnover experiments and steady-state triphosphatase activities are about threefold faster when 2′-*O*-Cy3-EDA-ATP is the substrate (Tables 1 and 2). On the other hand, the actin-activated triphosphatase rates for each of the Cy3 and Cy5 pairs of isomers were approximately the same, as judged by the product ratios being constant throughout the time course of the reaction. Bauer et al. (1997) have shown that the complex of mant-ADP and beryllium fluoride with subfragment 1 crystallizes specifically with 3′-*O*-mant-ADP bound under conditions that allow sufficient time for isomerization. As they point out, their result does not imply markedly different specificity in a solution of myosin for ribose-modified nucleotides. The kinetic differences between isomers interacting with myosin are less than have been found with GTP analogs and small G-proteins, which can show up to an order of magnitude difference in their kinetic interactions with 2′-*O*-mant-GTP and 3′-*O*-mant-GTP (Eccleston et al., 1991; Rensland et al., 1991).

The fluorescence properties of 2′- and 3′-*O*-Cy3-EDA-nucleotides show differences when free in solution and when bound to subfragment 1. Nevertheless, the relative differences are small when compared to 2′- and 3′-*O*-mant-GDP, the fluorescence of which differs by a factor of 2.5 (Rensland et al., 1991). The decrease we observe when 2′-*O*-Cy3-EDA-ATP binds to subfragment 1 contrasts with the much larger increase seen with the 3′ isomer (Fig. 3, *A* and *B*). Thus the signal from the 3′ isomer dominates when the mixed isomers interact with subfragment 1 in solution. Similarly, differences in fluorescence amplitudes occur when the ADP analogs bind to subfragment 1.

The fluorescent signals from the two isomers are expected to manifest themselves in a different way in TIRF ensemble and single-molecule studies. In TIRF microscopy it is the total fluorescence signal of the myosin-bound ATP or ADP analog that is recorded. Consider an example: the fluorescence of myosin-bound 2′-*O*-Cy3-EDA-ATP (steady-state complex) is equal to 87% of that of 2′-*O*-Cy3-EDA-ATP in solution (Fig. 3, *A* and *C*), while that of bound 3′-*O*-Cy3-EDA-ATP (steady-state complex) is 165% of that in solution (Fig. 3, *B* and *D*). In addition, the fluorescence of 3′-*O*-Cy3-EDA-ATP free in solution is only 89% of that of 2′-*O*-Cy3-EDA-ATP. This means that the Cy3 fluorescence of the myosin-bound 2′ isomer will be 59% of that of the 3′ isomer. Similar consideration of Fig. 3, *D* and *E*, shows that the fluorescence of myosin-bound 2′-*O*-Cy3-EDA-ADP is 82% that of the myosin-bound 3′-*O*-Cy3-EDA-ADP; the calculation was based on a K_d ($= K_4$) of 2.6 μM for the isomers to subfragment 1 (Table 1) and the fact that the fluorescence of the 2′ isomer in solution is 1.09 times that of the 3′ isomer. These percentages (59% and 82%) are the relevant ratios of the 2′- to 3′-Cy3 nucleotide fluorescences in the TIRF studies with myosin filaments. Note that we have so far been unable to address the relative fluorescence of 2′ and 3′ isomers in actomyosin studies or, indeed, the absolute fluorescence of any Cy3(Cy5)-nucleotide interacting with actomyosin. An important conclusion from this study is that certain single-molecule studies with Cy3-EDA-ATP (ADP) or any other ribose-modified nucleotide would benefit from the use of pure isomers.

Optically overlapping molecules on myosin filaments

We now address the issue of whether a fluorescent spot on myosin filaments might be due to more than one molecule of Cy3-nucleotide and the effect of multiple molecules on the kinetics. If the fluorescence intensity of a single molecule is well defined, its amplitude can be used; however, the fluorescences of myosin-bound 2′- and 3′-*O*-Cy3-EDA-ATP differ, and the Cy3 fluorescence will also vary because of variations in the distance of the fluorophore from the glass surface. The frequency of a fluorescent spot representing two or more bound molecules can also be considered theoretically. Images of single molecules are limited by the resolution of the microscope and video system employed for observation and recording. Each fluorophore is a very small light source, the emission dipole being on the order of 1 nm, so its image is the convolution of a point source with the point spread function of the microscope and the video system. The point spread function of a microscope is the spatial distribution of optical intensity in the image of a point source. This diffraction pattern consists of concentric bright and dark rings and is characterized by the diameter of the first dark ring, given by $d_o = 1.22\lambda/NA$, where λ is the wavelength of observation and *NA* is the numerical aperture of the objective. More than 83% of the total intensity is contained within this ring (Born and Wolf, 1997). In the present experiments with Cy3-EDA-ATP, λ is ~570 nm and $NA = 1.3$, giving $d_o = 535$ nm. However, the point spread function of the image intensifiers and CCD camera convolutes with that of our TIRF microscope to produce a broader total diameter, d_i, of 600 nm referred to the microscope's object space, containing more than 80% of the total intensity. Rayleigh's criterion for resolving two point sources gives a minimum separation of $d_i/2$ (i.e., 300 nm; Born and Wolf, 1997). Thus, if a single molecule is bound to a myosin filament, it will be indistinguishable spatially from any second molecule that binds within a circle of radius 300 nm. Neglecting the effect of the bare zone and assuming all binding sites are equally probable, there are on average 230 myosin heads within a circle of 300 nm radius centered on a given head of the 1000 in the 2.6-μm-long filament. The probability, p, of two or more molecules binding to the same filament within 300 nm is given by $p = 230P(n)/1000P(1)$, where $P(n)$ is the probability of two or more molecules (0.36) binding to a filament, and $P(1)$ is the probability (0.36) of the first molecule binding. Thus every time a single spot is observed, the probability of it arising from more than one Cy3 molecule during part of the observations is 23%. If we suppose (an extreme situation) that multiple binding events in a single spot overlap minimally (i.e., they are directly consecutive in time), simulation shows that true $1/\tau$ values will be 17% greater than measured $1/\tau$ values. In practice the error will be less than this, because in general multiple events will overlap in time. More comprehensive development of the theory has been done for single-channel recording (Colquhoun and Hawkes, 1995) but is not warranted here because of the low signal-to-noise ratio in the data.

Comparison of solution and TIRF kinetics

We now compare solution and TIRF kinetics, but first consider a problem with kinetic analysis involving myosin filaments. Measurements in the TIRF microscope of either single molecules or ensembles were made with synthetic filaments. Clearly the attachment of these filaments to the fused-silica surface, presumably through hydrophobic interactions, means that some myosin heads will be in contact with the surface and so may be restricted in their motion and/or

accessibility to ligands from the bulk solution, which in turn may affect the rate constants. Furthermore, most heads may not be able to interact with optimal stereochemistry for triphosphatase activation by F-actin and so may not exhibit full activity. Rate profiles in both Cy3-EDA-ATP and -ADP displacement experiments are biphasic with variable amplitudes. Despite this, single-molecule analyses have a distribution of dwell times that can be described as a single exponential decay, though, as already noted, the present series of experiments is limited to a time resolution of 270 ms.

2′- and 3′-O-Cy3(Cy5)-EDA-ATP

We now compare the kinetics of the solution, TIRF ensemble and single-molecule studies, various aspects of which are summarized in Table 2. Displacement rates of Cy3(Cy5)-EDA-ATP (steady-state complex) from a myosin filament by ATP can be equated with k_{cat} and agree with the values obtained with subfragment 1 in solution (Table 2), implying that an immobilized myosin filament has an ensemble triphosphatase activity similar to that of subfragment 1.

TIRF microscopy allows an ensemble assay of triphosphatase activity catalyzed by actin and myosin filaments that is not readily achieved under controlled conditions in solution. This preparation exhibits 3.5-fold activation of the Cy5-EDA-ATPase rate at 300 nM actin, where no activation at all would be seen in solution using solubilized myosin (e.g., subfragment 1) (cf. K'_m 61 μM, Table 1). The activation arises because the local concentration of actin in the vicinity of myosin is high because of rigor bond formation. Kinetics involving actin-myosin filaments in TIRF studies have been further elaborated by Bagshaw and co-workers (Bagshaw and Conibear, 1999; Sowerby et al., 1993).

The $1/\tau$ value of the fluorescence from individual Cy3 fluorophores on myosin fits the model of rapid binding of Cy3-EDA-ATP, followed by hydrolysis to Cy3-EDA-ADP as the rate-limiting step, with subsequent rapid dissociation of the products of cleavage. $1/\tau$ increased 3.2-fold with the addition of 600 nM actin. Thus the ensemble and single-molecule experiments each exhibited threefold F-actin activation of the myosin-filament triphosphatase rate.

Several issues complicate comparison between ensemble and single-molecule kinetics of triphosphatase activity (columns 5 and 6 of Table 2). First, even for pure isomers, the fluorescence decay associated with TIRF ensemble displacements was not described by a single exponential. This might be due in part to isoforms of myosin heavy and light chains having distinct triphosphatase activity and different fluorescence intensities of Cy3-EDA-ATP bound to the different myosin isoforms. Effects originating from this might not show up in solution studies where the observed signal depends on the difference between the fluorescence of protein-bound fluorophore and that of the free fluorophore in solution (though note the anomaly described in Fig. 2 *B*). Second, the complex time courses may also reflect a variable fraction of partially damaged myosins. In our experience, Mg^{2+}-dependent ATPase activity of damaged subfragment 1 often increases rather than decreases, for example, with aged protein solutions (data not shown), and a similar phenomenon may pertain here. Third, the anomaly of the severalfold higher single-molecule $1/\tau$ value with mixed 2′(3′)-*O*-Cy3-EDA-ATP isomers compared to the ensemble displacement rate may reflect in part the fact that all $1/\tau$ data with separated isomers were collected from later analyses with improved techniques.

When all of the above factors are taken into account, we believe that our data for Cy3-EDA-ATP show that ensemble and single-molecule studies report on the same biological process (i.e., Cy3-EDA-ATPase rate). Thus we do not suggest that differences are due to novel features of the triphosphatase mechanism being manifested in the single-molecule data. It follows that monitoring of single-molecule Cy3-EDA-ATPase activity by fluorescence as a function of mechanical properties of the actomyosin interaction, also being studied by single-molecule techniques, will give direct information about mechanochemical energy transduction. Previously this possibility has been severely limited for the vast majority of actomyosin systems that do not have the structural organization of striated muscle.

2′- and 3′-O-Cy3-EDA-ADP

2′- and 3′-*O*-Cy3-EDA-ADP dissociate from subfragment 1 with rate constants differing by a factor of only 1.4, so comparisons of Cy3-EDA-ADP interactions with subfragment 1 and myosin filaments were only made for mixed isomers. At 20°C, solution and TIRF ensemble kinetics were the same (cf. columns 4 and 5 of Table 2), while at 10°C the solution rate constant was smaller. The ensemble and single-molecule rates of 2′(3′)-*O*-Cy3-EDA-ADP dissociation from myosin filaments were the same within the SD of the data. Thus, as with the triphosphates, it appears that solution, TIRF ensemble, and single-molecule Cy3-EDA-ADP dissociation rates are the same to a first approximation. Hence it will be extremely interesting to widen these studies and to conduct strain- and temperature-dependent studies of Cy3-EDA-ADP dissociation from single cross-bridges.

Perspective

The separation of 2′- and 3′-*O*-Cy3-EDA-ATP(ADP) has permitted characterization of the elementary processes of their myosin subfragment 1 triphosphatase activities. The distinct kinetic and fluorescence properties of the two isomers mean that, if possible, it is better to work with one or other pure isomer; 3′-*O*-Cy3-EDA-ATP has the advantage of a greater fluorescence intensity difference between the isomer free in solution and that bound to subfragment 1 and of having an overall triphosphatase activity closer to that of ATP.

The near-identity of the rate constants of single-molecule and ensemble kinetics (Table 2), apart from the one case for which extraneous reasons may pertain, means that 3′-*O*-Cy3-EDA-ATP and 3′-*O*-Cy3-EDA-ADP are well suited to correlation of mechanical properties of single myosin molecules with elementary steps of myosin-nucleotide association and dissociation, and conformational changes, and of myosin-bound triphosphate hydrolysis and P_i dissociation. Furthermore, the results from Cy3-EDA-ADP serve as a model of what may occur in single-molecule receptor-ligand interactions. Nevertheless, much still has to be learned about the properties of 3′-*O*-Cy3-EDA-ATP(ADP) interacting with actomyosin. In addition, the time resolution of the single-molecule studies undertaken here has to be improved by two orders of magnitude to cover the time domain now accessible in corresponding mechanical studies (Veigel et al., 1999), but promise in this area is evident (Lu et al., 1998; Weiss, 1999; Xie and Trautman, 1998).

We thank Dr. S.A. Howell for determining mass spectroscopic data, Dr. M. J. Gradwell for recording NMR data, and the MRC Biomedical NMR Centre for access to facilities.

This work was supported by grants from the Hyogo Science and Technology Association, the Japan Science and Technology Corporation (Cooperative System for supporting Priority Research), the British Council, a grant-in-aid from the Ministry of Education, Science and Culture of Japan, and the MRC, UK.

REFERENCES

Alessi, D. R., J. E. T. Corrie, P. G. Fajer, M. A. Ferenczi, D. D. Thomas, I. P. Trayer, and D. R. Trentham. 1992. Synthesis and properties of a conformationally restricted spin-labeled analog of ATP and its interaction with myosin and skeletal muscle. *Biochemistry.* 31:8043–8054.

Anson, M. 1992. Temperature dependence and Arrhenius activation energy of F-actin velocity generated in vitro by skeletal myosin. *J. Mol. Biol.* 224:1029–1038.

Anson, M., D. R. Drummond, M. A. Geeves, E. S. Hennessey, M. D. Ritchie, and J. C. Sparrow. 1995. Actomyosin kinetics and in vitro motility of wild type *Drosophila* actin and the effects of two mutations in the Act88F gene. *Biophys. J.* 68:1991–2003.

Anson, M., and K. Oiwa. 1997. Design principles of instruments for kinetic studies with single fluorescent molecules. *Biophys. J.* 72:A180 (Abstr.).

Anson, M., and K. Oiwa. 1998. Signal-to-noise ratio, spatial and time resolution of measurements with single fluorescent molecules. *Biophys. J.* 74:A185 (Abstr.).

Anson, M., and K. Oiwa. 1999. Theoretical and practical considerations in selecting fluorophores for single molecule spectroscopy, imaging and kinetics. *Biophys. J.* 76:A448 (Abstr.).

Axelrod, D., T. P. Burghardt, and N. L. Thompson. 1984. Total internal reflection fluorescence. *Annu. Rev. Biophys. Bioeng.* 13:247–268.

Bagshaw, C. R., and P. B. Conibear. 1999. Single molecule enzyme kinetics: application to myosin ATPases. *Biochem. Soc. Trans.* 27:33–37.

Bagshaw, C. R., and D. R. Trentham. 1973. The reversibility of adenosine triphosphate cleavage by myosin. *Biochem. J.* 133:323–328.

Bauer, C. B., P. A. Kuhlman, C. R. Bagshaw, and I. Rayment. 1997. X-ray crystal structure and solution fluorescence characterization of Mg·2′(3′)-*O*-(*N*-methylanthraniloyl) nucleotides bound to the *Dictyostelium discoideum* myosin motor domain. *J. Mol. Biol.* 274:394–407.

Born, M., and E. Wolf. 1997. Principles of Optics, 6th Ed. Cambridge University Press, Cambridge.

Canepari, M., R. Rossi, M. A. Pellegrino, C. Reggiani, and R. Bottinelli. 1999. Speeds of actin translocation in vitro by myosins extracted from single rat fibres of different types. *Exp. Physiol.* 84:803–806.

Cheng, J. Q., W. Jiang, and D. D. Hackney. 1998. Interaction of mant-adenosine nucleotides and magnesium with kinesin. *Biochemistry.* 37: 5288–5295.

Colquhoun, D., and A. G. Hawkes. 1994. The interpretation of single channel recordings. *In* Microelectrode Techniques, 2nd Ed. D. Ogden, editor. The Company of Biologists Ltd., Cambridge. 141–188.

Colquhoun, D., and A. G. Hawkes. 1995. The principles of the stochastic interpretation of ion-channel mechanisms. *In* Single-Channel Recording, 2nd Ed. B. Sakmann and E. Neher, editors. Plenum, London. 397–482.

Conibear, P. B., and C. R. Bagshaw. 1996. Measurement of nucleotide exchange kinetics with isolated synthetic myosin filaments using flash photolysis. *FEBS Lett.* 380:13–16.

Conibear, P. B., D. S. Jeffreys, C. K. Seehra, R. J. Eaton, and C. R. Bagshaw. 1996. Kinetic and spectroscopic characterization of fluorescent ribose-modified ATP analogs upon interaction with skeletal muscle myosin subfragment 1. *Biochemistry.* 35:2299–2308.

Craig, R. 1977. Structure of A-segments from frog and rabbit skeletal muscle. *J. Mol. Biol.* 109:69–81.

Cremo, C. R., J. M. Neuron, and R. G. Yount. 1990. Interaction of myosin subfragment 1 with fluorescent ribose-modified nucleotides. A comparison of vanadate trapping and SH_1-SH_2 cross-linking. *Biochemistry.* 29:3309–3319.

Crowder, M. S., and R. Cooke. 1987. Orientation of spin-labeled nucleotides bound to myosin in glycerinated muscle fibers. *Biophys. J.* 51: 323–333.

Dexter, D. L. 1958. Theory of optical properties of imperfections in nonmetals. *Solid State Phys.* 6:353–411.

Dickson, R. M., A. B. Cubitt, R. Y. Tsien, and W. E. Moerner. 1997. On/off blinking and switching behaviour of single molecules of green fluorescent protein. *Nature.* 388:355–358.

Eccleston, J. F., K. J. M. Moore, G. G. Brownbridge, M. R. Webb, and P. N. Lowe. 1991. Fluorescence approaches to the study of the $p21^{ras}$ GTPase mechanism. *Biochem. Soc. Trans.* 19:432–437.

Eccleston, J. F., K. Oiwa, M. A. Ferenczi, M. Anson, J. E. T. Corrie, A. Yamada, H. Nakayama, and D. R. Trentham. 1996. Ribose-linked sulfoindocyanine conjugates of ATP: Cy3-EDA-ATP and Cy5-EDA-ATP. *Biophys. J.* 70:A159 (Abstr.).

Edman, K. A. P. 1979. The velocity of unloaded shortening and its relation to sarcomere length and isometric force in vertebrate muscle fibres. *J. Physiol. (Lond.).* 291:143–159.

Ellis-Davies, G. C. R., and J. H. Kaplan. 1994. Nitrophenyl-EGTA, a photolabile chelator that selectively binds Ca^{2+} with high affinity and releases it rapidly upon photolysis. *Proc. Natl. Acad. Sci. USA.* 91:187–191.

Faulstich, M., S. Zobely, G. Rinnerthaler, and J. V. Small. 1988. Fluorescent phallotoxins as probes for filamentous actin. *J. Muscle Res. Cell Motil.* 9:370–383.

Ferenczi, M. A., S. K. A. Woodward, and J. F. Eccleston. 1989. The rate of mant-ADP release from cross-bridges of single skeletal muscle fibers. *Biophys. J.* 55:441a (Abstr.).

Finer, J. T., R. M. Simmons, and J. A. Spudich. 1994. Single myosin molecule mechanics: piconewton forces and nanometre steps. *Nature.* 368:113–119.

Fromageot, H. P. M., B. E. Griffin, C. B. Reese, J. E. Sulston, and D. R. Trentham. 1966. Orientation of ribonucleoside derivatives by proton magnetic resonance spectroscopy. *Tetrahedron.* 22:705–710.

Funatsu, T., Y. Harada, M. Tokunaga, K. Saito, and T. Yanagida. 1995. Imaging of single fluorescent molecules and individual ATP turnovers by single myosin molecules in aqueous solution. *Nature.* 374:555–559.

Goody, R. S., W. Hofmann, and H. G. Mannherz. 1977. The binding constant of ATP to myosin S1 fragment. *Eur. J. Biochem.* 78:317–324.

Griffin, B. E., M. Jarman, C. B. Reese, J. E. Sulston, and D. R. Trentham. 1966. Some observations relating to acyl mobility in aminoacyl soluble ribonucleic acids. *Biochemistry.* 5:3638–3649.

Harada, Y., A. Noguchi, A. Kishino, and T. Yanagida. 1987. Sliding movement of single actin filaments on one-headed myosin filaments. *Nature.* 326:805–808.

Harada, Y., K. Sakurada, T. Aoki, D. D. Thomas, and T. Yanagida. 1990. Mechanochemical coupling in actomyosin energy transduction studied by in vitro movement assay. *J. Mol. Biol.* 216:49–68.

Hazlett, T. L., K. J. M. Moore, P. N. Lowe, D. M. Jameson, and J. F. Eccleston. 1993. Solution dynamics of $p21^{ras}$ proteins bound with fluorescent nucleotides: a time-resolved fluorescence study. *Biochemistry.* 32:13575–13583.

Hiratsuka, T. 1983. New ribose-modified fluorescent analogs of adenine and guanine nucleotides available as substrates for various enzymes. *Biochim. Biophys. Acta.* 742:496–508.

Hiratsuka, T. 1984. Distinct structures of ATP and GTP complexes in the myosin ATPase. *J. Biochem. (Tokyo).* 96:155–162.

Homsher, E., F. Wang, and J. Sellers. 1992. Factors affecting movement of F-actin filaments propelled by skeletal muscle heavy meromyosins. *Am. J. Physiol.* 262:C714–C723.

Ishijima, A., Y. Harada, H. Kojima, T. Funatsu, H. Higuchi, and T. Yanagida. 1994. Single-molecule analysis of the actomyosin motor using nanomanipulation. *Biochem. Biophys. Res. Commun.* 199:1057–1063.

Ishijima, A., H. Kojima, T. Funatsu, M. Tokunaga, H. Higuchi, H. Tanaka, and T. Yanagida. 1998. Simultaneous observation of individual ATPase and mechanical events by a single myosin molecule during interaction with actin. *Cell.* 92:161–171.

Jameson, D. M., and J. F. Eccleston. 1997. Fluorescent nucleotide analogs: synthesis and applications. *Methods Enzymol.* 278:363–390.

Kensler, R. W., and M. Stewart. 1993. The relaxed crossbridge pattern in isolated rabbit psoas muscle thick filaments. *J. Cell Sci.* 105:841–848.

Kron, S. J., and J. A. Spudich. 1986. Fluorescent actin filaments move on myosin fixed to a glass surface. *Proc. Natl. Acad. Sci. USA.* 83:6272–6276.

Kuhlman, P. A., and C. R. Bagshaw. 1998. ATPase kinetics of *Dictyostelium discoideum* myosin II motor domain. *J. Muscle Res. Cell Motil.* 19:491–504.

Lu, H. P., L. Xun, and X. S. Xie. 1998. Single-molecule enzymatic dynamics. *Science.* 282:1877–1882.

Mahmood, R., C. Cremo, K. L. Nakamaye, and R. G. Yount. 1987. The interaction and photolabeling of myosin subfragment 1 with 3′(2′)-*O*-(4-benzoyl)benzoyladenosine 5′-triphosphate. *J. Biol. Chem.* 262: 14479–14486.

Margossian, S. S., and S. Lowey. 1982. Preparation of myosin and its subfragments from rabbit skeletal muscle. *Methods Enzymol.* 85:55–71.

Mehta, A. D., R. S. Rock, M. Rief, J. A. Spudich, M. S. Mooseker, and R. E. Cheney. 1999. Myosin-V is a processive actin-based motor. *Nature.* 400:590–593.

Millar, N. C., and M. A. Geeves. 1983. The limiting rate of ATP-mediated dissociation of actin from rabbit skeletal myosin subfragment 1. *FEBS Lett.* 160:141–148.

Moisescu, D. G. 1976. Kinetics of reaction in calcium-activated skinned muscle fibres. *Nature.* 262:610–613.

Molloy, J. E., J. E. Burns, J. Kendrick-Jones, R. T. Tregear, and D. C. S. White. 1995. Movement and force produced by a single myosin head. *Nature.* 378:209–212.

Mujumdar, R. B., L. A. Ernst, S. R. Mujumdar, C. J. Lewis, and A. S. Waggoner. 1993. Cyanine dye labeling reagents: sulfoindocyanine succinimidyl esters. *Bioconjug. Chem.* 4:105–111.

Nagashima, H. 1986. Active movement of synthetic myosin filaments observed by dark-field light microscopy. *J. Biochem. (Tokyo).* 100: 1023–1029.

Nie, S., and R. N. Zare. 1997. Optical detection of single molecules. *Annu. Rev. Biophys. Biomol. Struct.* 26:567–596.

Oiwa, K., M. Anson, J. F. Eccleston, and D. R. Trentham. 1998. Isolation and characterization of 2′-*O*- and 3′-*O*-isomers of Cy3-EDA-ATP: kinetics and single molecule studies. *Biophys. J.* 74:A260 (Abstr.).

Oiwa, K., M. Anson, J. F. Eccleston, and D. R. Trentham. 1999. Kinetics of myosin ATPase studies by TIRF microscopy with separated 2′- and 3′-*O*-Cy3-EDA-ATP at the level of single molecules. *Biophys. J.* 76: A166 (Abstr.).

Oiwa, K., M. Anson, J. F. Eccleston, A. Yamada, H. Nakayama, and D. R. Trentham. 1997. Microscopic kinetic measurements of single Cy3-EDA-ADP molecules interacting with myosin filaments in vitro. *Biophys. J.* 72:A180 (Abstr.).

Oiwa, K., M. Anson, A. Yamada, J. F. Eccleston, J. E. T. Corrie, M. A. Ferenczi, D. R. Trentham, and H. Nakayama. 1996. Microscopic observations of Cy3-EDA-ATP and Cy5-EDA-ATP binding to myosin filaments in vitro. *Biophys. J.* 70:A159 (Abstr.).

Oiwa, K., G. P. Reid, C. T. Davis, J. F. Eccleston, J. E. T. Corrie, and D. R. Trentham. 1995. 2′- and 3′-carbamoyl derivatives of adenine nucleotides: their rates of interconversion and activity as substrates in ATP and ADP utilizing enzymes. *Biophys. J.* 68:A64 (Abstr.).

Onur, G., G. Schäfer, and H. Strotmann. 1983. Synthesis of 2′-/3′-*O*-acylated adenine nucleotide analogs and their interactions in photophosphorylation. *Z. Naturforsch.* 38c:49–59.

Pardee, J. D., and J. A. Spudich. 1982. Purification of muscle actin. *Methods Enzymol.* 85:164–181.

Rensland, H., A. Lautwein, A. Wittinghofer, and R. S. Goody. 1991. Is there a rate-limiting step before GTP cleavage by H-*ras* p21? *Biochemistry.* 30:11181–11185.

Rice, S. O. 1954. Mathematical analysis of random noise. *In* Selected Papers on Noise and Stochastic Processes. N. Wax, editor. Dover Publications, New York. 133–294.

Sowerby, A. J., C. K. Seehra, M. Lee, and C. R. Bagshaw. 1993. Turnover of fluorescent nucleoside triphosphates by isolated immobilized myosin filaments. Transient kinetics on the zeptomole scale. *J. Mol. Biol.* 234:114–123.

Thirlwell, H., J. E. T. Corrie, G. P. Reid, D. R. Trentham, and M. A. Ferenczi. 1994. Kinetics of relaxation from rigor of permeabilized fast-twitch fibers from the rabbit using a novel caged ATP and apyrase. *Biophys. J.* 67:2436–2447.

Thirlwell, H., J. A. Sleep, and M. A. Ferenczi. 1995. Inhibition of unloaded muscle shortening velocity in permeabilised muscle fibres by caged ATP compounds. *J. Muscle Res. Cell Motil.* 16:131–137.

Tonomura, Y. 1973. ATP analogues. *In* Muscle Proteins, Muscle Contraction and Cation Transport. University Park Press, Tokyo. 257–271.

Toyoshima, Y. Y., S. J. Kron, E. M. McNally, K. R. Niebling, C. Toyoshima, and J. A. Spudich. 1987. Myosin subfragment-1 is sufficient to move actin filaments in vitro. *Nature.* 299:557–559.

Toyoshima, Y. Y., S. J. Kron, and J. A. Spudich. 1990. The myosin step size: measurement of the unit displacement per ATP hydrolyzed in an in vitro assay. *Proc. Natl. Acad. Sci. USA.* 87:7130–7134.

Trentham, D. R., J. F. Eccleston, and C. R. Bagshaw. 1976. Kinetic analysis of ATPase mechanisms. *Q. Rev. Biophys.* 9:217–281.

Uyeda, T. Q. P., S. J. Kron, and J. A. Spudich. 1990. Myosin step size estimation from slow sliding movement of actin over low densities of heavy meromyosin. *J. Mol. Biol.* 214:699–710.

Veigel, C., L. M. Coluccio, J. D. Jontes, J. C. Sparrow, R. A. Milligan, and J. E. Molloy. 1999. The motor protein myosin-I produces its working stroke in two steps. *Nature.* 398:530–533.

Warshaw, D. M., E. Hayes, D. Gaffney, A-M. Lauzon, J. Wu, G. Kennedy, K. Trybus, S. Lowey, and C. Berger. 1998. Myosin conformational states determined by single fluorophore polarization. *Proc. Natl. Acad. Sci. USA.* 95:8034–8039.

Weeds, A. G., and R. S. Taylor. 1975. Separation of subfragment-1 isoenzymes from rabbit skeletal muscle myosin. *Nature.* 257:54–56.

Weiss, S. 1999. Fluorescence spectroscopy of single biomolecules. *Science.* 283:1676–1683.

Woodward, S. K. A., J. F. Eccleston, and M. A. Geeves. 1991. Kinetics of the interaction of 2′(3′)-*O*-(*N*-methylanthraniloyl)-ATP with myosin subfragment 1 and actomyosin subfragment 1: characterization of two acto-S1-ADP complexes. *Biochemistry.* 30:422–430.

Xie, X. S., and J. K. Trautman. 1998. Optical studies of single molecules at room temperature. *Annu. Rev. Phys. Chem.* 49:437–476.

Xu, G., and J. S. Evans. 1996. The application of "excitation sculpting" in the construction of selective one-dimensional homonuclear coherence-transfer experiments. *J. Magn. Reson. B.* 111:183–185.